Modelling Tsunami Runup on Three-Island Groups

by

Selina Tan (JN)

Fourth-year undergraduate project
in Group D, 2012/2013

Supervised by Dr. D. Liang

I hereby declare that, except where specifically indicated, the work submitted herein is my own original work.

ABSTRACT

Extensive damage can be caused by major tsunami events particularly in the Pacific Ocean. The behaviour exhibited by an extreme wave as it interacts with clusters of islands can be somewhat unexpected and it is important to investigate this effect in order to eliminate or minimise the destruction caused. This report examines the application of a Boussinesq-type model to study the interaction between a propagating solitary wave, representative of a tsunami wave, and clusters of three idealised conical islands, similar to those found in the Pacific Ocean. The shallow-water Boussinesq-type equations are solved in the model using the shock-capturing time variation diminishing (TVD) Lax-Wendroff scheme, the accuracy of which is validated against experimental data obtained for a single conical island. A comparison between the experimental and numerical time series provides sufficient supportive evidence to deem the model reliable for the purposes of computing the distribution of run-up. In this study, the interaction behaviour of the wave on the three-island cluster is analysed with particular focus on the maximum run-up heights predicted for each island and the effects of two variable parameters: the normalised island separation between adjacent islands, and the angle of rotation of the cluster configuration. Simulations are undertaken for a variety of combinations of island spacing and angle of rotation. Each combination is categorised as partially merged at still water level, partially merged below still water level, or completely separated, depending on the spacing. For each simulation, the magnitudes and locations of maximum run-up heights are obtained for each island, and the variations analysed. These two free parameters are found to have a significant influence on the predicted run-up heights for each island.

At small separations, for partially merged island clusters, relatively large run-up heights are predicted within the narrow channels between islands. This behaviour is attributable to the effects of non-linear wave reflection, refraction, diffraction and shoaling effects. It is observed that at particularly small separations, the cluster of islands becomes comparable to a single island entity, as the close proximity of the islands disrupts the propagating wave, preventing it from continuing past the islands and producing one wake in the process. At larger separations, however, the individual islands exhibit increasingly similar behaviour to that of isolated islands with a reduction in the interaction channel effects between adjacent islands. As the rotation of the cluster arrangement varies, the prominence of the shadow effect fluctuates. As the downstream island moves into the shadow of the upstream islands, it experiences reduced exposure to the direct impact of the incident wave

and therefore sees less run-up. The extent of this exposure of the downstream island is also affected by the separation of the islands, which determines whether the island lies in the sheltered regions of both of the upstream islands.

Although the analysis in this study is heavily simplified through the use of idealised conical islands, identical in size, this study provides a significant insight into the propagation behaviour of a solitary wave impacting on a cluster of three islands. It provides useful information for the purposes of planning tsunami wave mitigation actions, designing and implementing coastal defence structures and informing on clearance requirements for coastal construction. In this way, it shall be possible to extensively reduce the damage caused by these extreme wave events.

CONTENTS

1. INTRODUCTION

The impact of a large tsunami on islands and their inhabitants can be devastating. The destructive nature of this hazardous natural phenomenon has been demonstrated by past tsunami events, many of which have occurred in the Pacific Ocean, including the recent tsunami to hit the Pacific coast of Japan in 2011, killing almost 19,000 people. The objective of this study is to investigate the impact of a tsunami wave on small islands, such as those found in the Pacific Ocean. The behaviour of a tsunami wave as it attacks a single island can demonstrate unexpected behaviour in terms of anticipated run-up around the island. As the wave approaches, large run-up is observed on the front of the island, as expected, and a reflected wave radiates out in a circular configuration away from the island. However, refraction and diffraction also cause the incident wave to bend around the island, forming edge waves. In the case of a single island, due to the symmetry of the oncoming wave and the island itself, the edge waves wrap evenly around the perimeter of the island, meeting again at the rear and as a result, creating relatively large run-up on the leeside, as would not necessarily be expected.

Wave propagation is a complex process to model due to various non-linear wave effects, and is made even more complicated by the effect of clusters of islands. The arrangement of these clusters of islands with regards to the spacing and the orientation can cause interesting interaction effects between the incident wave and reflected waves, impacting on the run-up heights recorded for each island. For modelling purposes, a solitary wave is used as representative of a tsunami, and an idealised flat-topped cone as representative of a conical island. Past research has been carried out on the effects of a propagating solitary wave on a single island and the analysis applied to the case of two-island clusters, concluding that the interference between neighbouring islands plays a significant role in determining the interaction behaviour of the waves and therefore the maximum run-up height observed on any one of the islands. It was discovered that with sufficient separation, the islands had minimal interference with the resulting measurements of run-up, and could be treated as effectively isolated islands. This paper aims to extend this research to three-island clusters with varying geometrical configurations and observing the resulting interaction effects.

Ultimately, the significance of this project is to provide useful information on the mitigation of tsunami waves in relation to its impact on small islands. Modelling these effects and the possible outcomes of a tsunami can contribute to the future planning and development of coastal settlements and defences, particularly on small islands in the Pacific Ocean, in order to significantly reduce the damage caused to thousands of lives. The most suitable locations for construction can be determined by finding the areas most vulnerable to the action of the waves. Raising awareness of the likely damage caused in the event of a tsunami wave and predicting the extent of its destruction can prepare people for the consequences of the natural disaster, allowing them to effectively manage their property to ensure the best outcome with minimal loss of life.

2. THEORETICAL BASIS

2.1. Theoretical development

2.1.1. Shallow Water Equations

The propagation of a tsunami wave can be modelled numerically using the Shallow Water Equations, derived as the depth-averaged form of the Navier-Stokes equation (*Chen and Liang, 2012*), which describes the motion of fluid substances. In the case of deep ocean tsunamis, often characterised as water depths of greater than 30m, a fast-moving tsunami is assumed to have an amplitude much smaller than the water depth. The friction on the seabed and the convective inertia terms are assumed to be negligible so the wave can be modelled using linear shallow water approximations (*Wang, 2009*). However, as the tsunami wave propagates over the continental shelf and into coastal areas, characterised as water depths of between 2m and 30m, the linear shallow water equations are no longer valid, as factors such as seabed friction and convective inertia affect the flow of the wave. The wavelength reduces and the amplitude increases as the wave moves into shallow water. In this region, the Coriolis force due to the rotation of the Earth can be taken as negligible (*Wang, 2009*). Frequency dispersion is another significant factor that must be accounted for if the distance travelled by the tsunami is long. This frequency dispersion effect is created by waves of varying wavelengths propagating at different phase velocities. The non-linear Shallow Water Equations can then be represented in Cartesian coordinates in the following form (*Liang, Lin and Falconer, 2007*):

$$\frac{\partial \eta}{\partial t} + \frac{\partial p}{\partial x} + \frac{\partial q}{\partial y} = 0 \tag{1}$$

$$\frac{\partial p}{\partial t} + \frac{\partial}{\partial x}\left(\frac{p^2}{d}\right) + \frac{\partial}{\partial y}\left(\frac{pq}{d}\right) + gd\frac{\partial \eta}{\partial x} + F_x = 0 \tag{2}$$

$$\frac{\partial q}{\partial t} + \frac{\partial}{\partial x}\left(\frac{pq}{d}\right) + \frac{\partial}{\partial y}\left(\frac{q^2}{d}\right) + gd\frac{\partial \eta}{\partial y} + F_y = 0 \tag{3}$$

where η is the water free-surface elevation, the total water depth $d = \eta + h$, and h is the still-water depth. p and q are defined as the horizontal components of the volume flux in the X and Y directions respectively. In equations (2) and (3), the terms F_x and F_y represent the bottom frictional effects, evaluated by using Manning's formula as follows:

$$F_x = \frac{gn^2}{d^{7/3}} p(p^2 + q^2)^{1/2} \tag{4}$$

$$F_y = \frac{gn^2}{d^{7/3}} q(p^2 + q^2)^{1/2} \tag{5}$$

where n is the Manning's relative roughness coefficient.

2.1.2. Boussinesq Model

A range of physical wave effects are accurately reproduced by numerical models based on Boussinesq-type equations (*Madsen and Sørensen, 1992*) including refraction, diffraction, reflection of irregular, finite-amplitude waves propagating over complex bathymetries, and shoaling. The Boussinesq-type model is used for large regions near shore as an extension of the Shallow Water Equations for long-wave non-linear theory taking wave dispersion effects into consideration. The wave frequency dispersion effect is introduced to the Shallow Water flow equations by taking into account the effect that the vertical accelerations and curvature of the streamlines have on the pressure distribution (*Madsen, Murray and Sorensen, 1991*). Modifications have been made to the Boussinesq equations to model linear dispersion characteristics accurately and to ensure that the equations are valid on a slowly varying bathymetry. The shallow-water Boussinesq-type equations can be represented in the following matrix-vector form:

$$\mathbf{X}_t + \mathbf{F}_x + \mathbf{G}_y = \mathbf{S} + \mathbf{T} \tag{6}$$

where the subscripts *t, x,* and *y* denote differentiation with respect to time and the x- and y-spatial coordinates, and the vectors are defined as:

$$\mathbf{X} = \begin{bmatrix} \eta \\ p \\ q \end{bmatrix} \qquad \mathbf{F} = \begin{bmatrix} p \\ \frac{p^2}{d} + \frac{g\eta^2}{2} + gh\eta \\ \frac{pq}{d} \end{bmatrix} \qquad \mathbf{G} = \begin{bmatrix} q \\ \frac{pq}{d} \\ \frac{q^2}{d} + \frac{g\eta^2}{2} + gh\eta \end{bmatrix} \tag{7a,b,c}$$

$$\mathbf{S} = \begin{bmatrix} 0 \\ g\eta h_x - \frac{n^2 gp\sqrt{p^2 + q^2}}{d^{7/3}} + \varphi \\ 0 \end{bmatrix} \qquad \mathbf{T} = \begin{bmatrix} 0 \\ 0 \\ g\eta h_y - \frac{n^2 gq\sqrt{p^2 + q^2}}{d^{7/3}} + \psi \end{bmatrix} \tag{7d,e}$$

The additional Boussinesq dispersive terms, φ and ψ, found in Equations (7d) and (7e), have then been defined as follows (*Liang, Borthwick and Romer-Lee, 2012*):

$$\varphi = \left(B + \frac{1}{3}\right) h^2 \left(p_{xxt} + q_{xyt}\right) + Bgh^3 \left(\eta_{xxx} + \eta_{xyy}\right) + hh_x \left(\frac{1}{3} p_{xt} + \frac{1}{6} q_{yt} + 2Bgh\eta_{xx} + Bgh\eta_{yy}\right) + hh_y \left(\frac{1}{6} q_{xt} + Bgh\eta_{xy}\right) \tag{8}$$

$$\psi = \left(B + \frac{1}{3}\right) h^2 \left(q_{yyt} + p_{xyt}\right) + Bgh^3 \left(\eta_{yyy} + \eta_{xxy}\right) + hh_y \left(\frac{1}{3} q_{yt} + \frac{1}{6} p_{xt} + 2Bgh\eta_{yy} + Bgh\eta_{xx}\right) + hh_x \left(\frac{1}{6} p_{yt} + Bgh\eta_{xy}\right) \tag{9}$$

where B is the dispersion coefficient and equals 1/15.

2.1.3. Total variation diminishing (TVD) Lax-Wendroff Scheme

The formation and propagation of shocks in free surface flows poses a significant challenge for numerical schemes intended to solve the Shallow Water Equations, as it generates a change in the vertical flow conditions. The main difficulty is in locating the exact position of the sharp change in the flow induced by the shock, as it is inevitable that it will occur within a grid interval, despite how fine the grid size is (*Liang, Lin and Falconer, 2007*). A shock-capturing approach is adopted to identify and track the shocks accurately in an unsteady flow situation. It incorporates a solution strategy over the entire domain, irrespective of discontinuities in the flow or regions of smooth flow. In this way, the shock-capturing method is deemed more reliable than the alternative shock-fitting method, which works by isolating the shock from the adjacent smooth regions of flow, and instead of analysing the domain as a whole, it treats the shock as a separate internal moving boundary. This limits the number of shocks that can be detected and the direction of the shocks to be tracked, a problem not encountered by the shock-capturing method (*Liang, Lin and Falconer, 2007*).

The total variation diminishing (TVD) Lax-Wendroff scheme is a robust shock-capturing numerical model used to solve the shallow-water Boussinesq-type equations as outlined in Section 2.1.2. The basis of the overall solution involves the operator-splitting technique, whereby the solution of the shallow-water Boussinesq-type equations is found by solving one-dimensional equations. For the purposes of explaining the TVD numerical scheme, the following one-dimensional equation describing the variation in flow in the x-direction is considered (*Liang, Lin and Falconer, 2007*):

$$\frac{\partial U}{\partial t}+\frac{\partial F}{\partial x}=S \tag{10}$$

where U represents η, q_x or q_y; F is the flux term and S is the source term.

Equation (10) is hence solved using the Lax-Wendroff finite difference scheme to step from $\mathbf{U}^{n}$ to $\mathbf{U}^{n+1}$. The model consists of a time-stepping scheme using finite differences as illustrated in Fig. 1 (*Liang, Borthwick and Romer-Lee, 2012*).

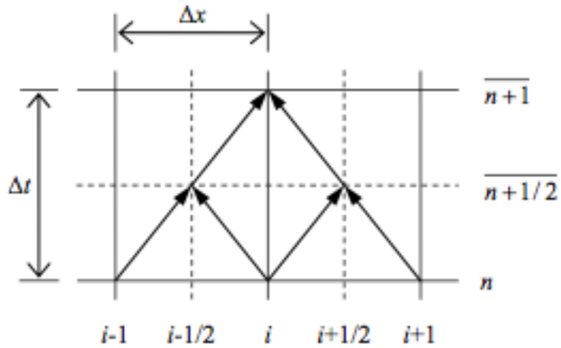

Fig. 1 Two-step Lax-Wendroff scheme, Liang et al. (2012)

The two-step Lax-Wendroff scheme consists of two stages. The first stage involves using space-centred differencing and time-forward differencing to calculate the values at half time steps $\left(\frac{\Delta t}{2}\right)$ and half grid points $\left(\frac{\Delta x}{2}\right)$. The second step involves using centred differencing in time and space in the following form:

$$\mathbf{U}_{i+1/2}^{\overline{n+1/2}}=\frac{1}{2}\left(\mathbf{U}_{i+1}^{n}+\mathbf{U}_{i}^{n}\right)-\frac{\Delta t}{2\Delta x}\left(\mathbf{F}_{i+1}^{n}-\mathbf{F}_{i}^{n}\right)+\frac{\Delta t}{4}\left(\mathbf{S}_{i+1}^{n}+\mathbf{S}_{i}^{n}\right) \tag{11a}$$

$$\mathbf{U}_{i}^{\overline{n+1}}=\mathbf{U}_{i}^{n}-\frac{\Delta t}{\Delta x}\left(\mathbf{F}_{i+1/2}^{\overline{n+1/2}}-\mathbf{F}_{i-1/2}^{\overline{n+1/2}}\right)+\frac{\Delta t}{2}\left(\mathbf{S}_{i+1/2}^{\overline{n+1/2}}+\mathbf{S}_{i-1/2}^{\overline{n+1/2}}\right) \tag{11b}$$

A full time-step, however, is only achieved after an additional symmetric TVD term is added with the purpose of evaluating the smoothness of the solution. Where the solution is found to vary steeply with a sharp gradient, diffusion is introduced to remove the numerical oscillations (*Liang, Lin and Falconer, 2007*). The TVD amendment of Equations (11*a*) and (11*b*) is then as follows:

$$\mathbf{U}_{i}^{n+1}=\mathbf{U}_{i}^{\overline{n+1}}+\left[G(r_{i}^{+})+G(r_{i+1}^{-})\right]\cdot\Delta\mathbf{U}_{\mathbf{i+1/2}}^{\mathbf{n}}-\left[G(r_{i-1}^{+})+G(r_{i}^{-})\right]\cdot\Delta\mathbf{U}_{\mathbf{i-1/2}}^{\mathbf{n}} \tag{12}$$

where

$$\Delta \mathbf{U}_{i+1/2}^{n} = \mathbf{U}_{i+1}^{n} - \mathbf{U}_{i}^{n} \tag{13}$$

$$r_i^{+} = \frac{\langle \Delta \mathbf{U}_{i-1/2}^{n}, \Delta \mathbf{U}_{i+1/2}^{n} \rangle}{\langle \Delta \mathbf{U}_{i+1/2}^{n}, \Delta \mathbf{U}_{i+1/2}^{n} \rangle} \tag{14a}$$

$$r_i^{-} = \frac{\langle \Delta \mathbf{U}_{i-1/2}^{n}, \Delta \mathbf{U}_{i+1/2}^{n} \rangle}{\langle \Delta \mathbf{U}_{i-1/2}^{n}, \Delta \mathbf{U}_{i-1/2}^{n} \rangle} \tag{14b}$$

The point brackets in Equations (14*a*) and (14*b*) represent the scalar product of the two vectors within the brackets. The function, $G(r_i)$, is then defined as follows:

$$G(r_i) = 0.5 \times C_i \times [1 - \phi(r_i)] \tag{15}$$

The function, $\phi(r_i)$, is defined as the non-linear flux limiter as follows:

$$\phi(r_i) = \max\big(0, \min(2r_i, 1)\big) \tag{16}$$

The parameter, C_i, in Equation (15) is dependent on the local Courant number, Cr_i, and is defined as:

$$C_i = \begin{cases} Cr_i \times (1 - Cr_i), & \text{if } Cr_i \leq 0.5 \\ 0.25, & \text{else} \end{cases} \tag{17}$$

$$Cr_i = \frac{\left(|p_i/d_i| + \sqrt{gd_i}\right)\Delta t}{\Delta x} \tag{18}$$

The standard TVD Lax-Wendroff scheme has the benefit of second-order accuracy in time and space and is applied to solve the shallow water Boussinesq-type equations (*Liang, 2010*).

2.2. Previous application of model

The theory outlined in Section 2.1 is implemented in modelling the propagation of a solitary wave and its effect on a single island and on clusters of islands. For the case of the single island, the numerical model of the TVD Lax-Wendroff scheme has been validated against laboratory experimental measurements previously recorded by *Liu et al. (1995)*, demonstrating significant accuracy in the modelling of the tsunami wave. It can be concluded that the model has the capability to simulate the complex processes that occur as the propagating solitary waves come into contact with the single conical island. Before simulating the three-island cluster scenario, the numerical model will again be verified against experimental data for the single island case to ensure that the analysis can be used to accurately model the three-island cluster.

Previous research has investigated the impact of a solitary tsunami wave on two-island clusters with varying geometry and configurations, discovering interesting results associated with the interaction behaviour between the wave and the islands (*Liang, Borthwick and Romer-Lee, 2012*). Depending on the geometrical arrangement of the islands with regards to the spacing and the orientation relative to the direction of the incident wave, reflected waves are generated as the incident wave collides with the island located downstream of the wave source. The behaviour of these reflected waves and the possible interaction with the incident wave could significantly impact on the maximum run-up heights recorded for each island.

The application of the numerical model to the simulation of the propagating wave has highlights another significant observation called the '*shadow effect*'. This effect is most noticeable when the downstream island is located directly behind the upstream island. If the wake of the upstream island extends a long distance, the downstream island can experience a substantial reduction in the run-up height recorded. Findings from *Chen and Liang (2011)* suggest that the shadow effect acts in a wedge downstream of the island, sweeping roughly 25° from the centreline of the island on either side. As the downstream island moves out of the sheltered region, however, the shadow effect becomes insignificant and high run-up is again recorded on the upstream side of the island in question.

The separation of the islands is a major contributing factor in determining the maximum run-up heights recorded. If the islands are sufficiently separated, the wave-wave interaction factor between the incident wave and the reflected waves becomes less significant and the simulation can resemble single island behaviour. At small separations, the islands can either be completely merged together, and therefore act as one large single island, or connected only under the still water level. In the latter case, complex wave transformation processes occur in the narrow channel between the two islands that can result in unexpectedly high run-up measurements.

These effects are likely to be observed in the three-island cluster simulations, and in some cases are likely to be amplified by the presence of the third island.

3. COMPUTATIONAL CONDITIONS

3.1. Initial conditions of computational setup

For the purposes of verifying the numerical predictions of the shallow water Boussineq-type model against the experimental results, the initial conditions of the model and the computational setup are chosen to replicate the experimental setup. In *Liu et al. (1995)*'s large-scale laboratory experiment undertaken, a rectangular wave basin of 30m wide, 25m long and 60cm deep was used. Waves were created in the tank by a horizontal wave generator with 60 different paddles, each of which was 46cm wide and moving independently. Wave absorbers were installed along the four basin sides to minimise wave reflections and to remove any boundary effects on the measured run-up height. In the computational setup, the wave absorbers are incorporated in the model by expanding the computational domain to 50m long and 50m wide to ensure that boundary effects are sufficiently eliminated during the simulation. The boundaries, excluding the wave-generating boundary, are also defined as linear transmissive boundaries by setting the normal derivatives of all variables as zero. Combined with the expanded computational domain, this prevents interference from any unwanted disturbances produced by boundary reflections.

Input conditions for the experimental first order solitary wave are specified with an amplitude of 0.032m moving through the basin of still water depth of 0.32m. For wave propagation over such short distances as in the laboratory experiment, the bottom friction effect is assumed to be negligible. This was accommodated in the experiment through the use of smooth concrete for the construction of the surface of the island and the wave basin. In the computational setup, the Manning's roughness coefficient, n, is specified as 1×10^{-10} s/m$^{1/3}$. An isolated flat-topped concrete cone was used to represent the single island in the experiment with a height of 0.625m, a crest radius of 1.1m, a base radius of 3.6m, a radius of 2.32m at still water level, and a 1:4 slope (*Fig. 2*). For the simulations, a grid spacing of $\Delta x = \Delta y = 0.05$m and a time step of $\Delta t = 0.01$s are sufficient.

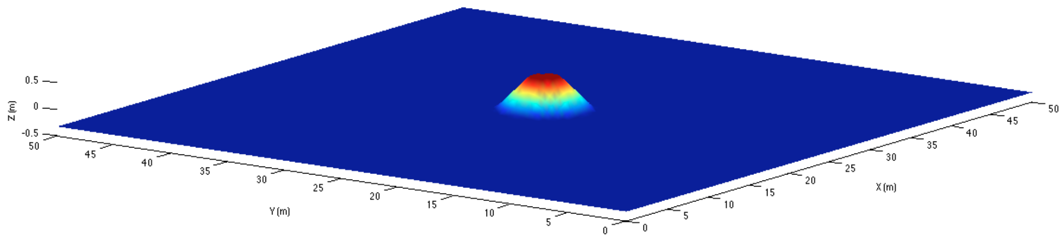

Fig. 2 Computational setup of wave basin and single conical island

3.2. Wetting and drying technique

As part of the computational framework, the moving boundary associated with the incident wave attacking the island is modelled using an empirical method. This allows for continuous wetting and drying to ensure that the boundary of the water and the land is accurately simulated during the wave run-up (*Liang, Borthwick and Romer-Lee, 2012*). At each time step, a drying check and a wetting check is conducted for each node. The water depth is calculated at each node, and in the drying check, the node is considered to be dry if the water depth is less than 1mm, and is then excluded from the computation until it is considered wet again. In the wetting check, the *frozen water level* is defined as the level of water above a given dry node, and is compared with the *free water level*, defined as the highest level of water of any wet nodes adjacent to the node in question. If the free water level is found to be greater than 2mm higher than the frozen water level, then a layer of 1mm of water is shifted from the wet node to the dry node in order to maintain the overall mass balance (*Liang, Lin and Falconer, 2007*). Consequently, the previously dry node may now be considered wet and is therefore included in the following computation. This continues for each node and at each time step during the simulation.

The stability of the computational method is improved through the use of a threshold water depth, specified as 5mm. Below this depth, the wave frequency dispersion terms are switched off and the local shallow-water equations are then solved instead. This approach is particularly effective as it eliminates any numerical complications associated with the creation of negative still water depths during wave run-up. In the numerical model, a condition of no flow is imposed at the wet and dry boundary to guarantee a mass balance in the flow. The TVD flux component between the identified wet and dry nodes is also specified as zero. Comprehensive computational experiments using this numerical method have proven that the wetting and drying technique outlined here is capable of satisfying the requirement for mass conservation, and is therefore an appropriate model to use for the purpose of simulating tsunami wave propagation and island run-up.

3.3. Computational procedure

3.3.1. Preparation of input data

Prior to simulating wave propagations, the initial input topography data for each node in the domain is prepared using MATLAB. For verification of the numerical model using the single island simulation, the centre of the island is located at the centre of the 50m x 50m computational domain. The variables, z, h, and η, are then defined in MATLAB as the depth of the bed, still water depth and the free-surface displacement, respectively, for each node of the domain. If the node is located outside of the outer perimeter of the bottom of the island, the variable, z, is taken as the negative value of the still water depth (= –0.32m) and η is taken as zero. If the node is located within the crest perimeter of the island, the variables, z and η, are taken as the height from the still water level to the top surface of the island. Otherwise, if the node is located on the slope of the island, the variables are calculated depending on whether the node is on the submerged part of the slope, i.e. below the still water level, or on the dry part of the slope. An input data file is produced with the initial conditions for each node specifying the variables, h (= −z), η, QXp and QXq (the input flux conditions), and Manning's roughness coefficient, n. Refer to the Appendix for further details of the MATLAB script.

For the case of the three-island cluster simulation, the centre of the three-island arrangement is located at the centre of the computational domain and the islands are defined as in *Fig. 3*. The parameter, S, is the island separation and θ is the angle of rotation of Island 1 relative to the direction of the incident wave.

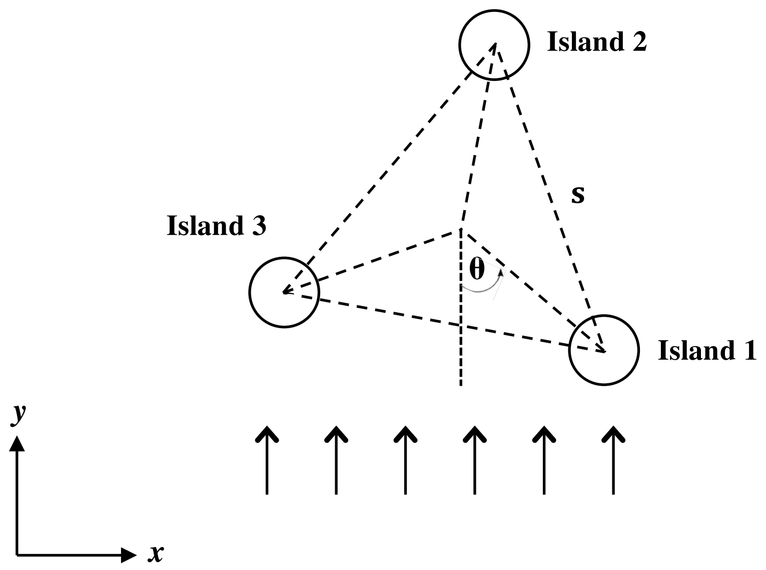

Fig. 3 Plane view of solitary wave interaction with the three-island cluster

Due to the multitude of possible configurations for the three-island case, using islands of uniform size and maintaining an equilateral triangle formation for each simulation simplify the analysis. The non-dimensional normalised variable, S/d, is defined with d being the diameter of the islands at still water level, taken as 4.64 m. Simulations are run for varying configurations, initially, by increasing S/d from 1 to 3 in intervals of 0.5. Due to rotational symmetry, arrangements of 0° ≤ θ ≤ 60° are equivalent to the arrangements of 60° ≤ θ ≤ 120°.

To avoid repeating simulations, θ is hence only varied between 0° and 60° in intervals of 15° initially. Similar to the single island case, the input variables, z, h and η, are defined in MATLAB for each node. This involves, first, determining the co-ordinates of the centres of the three islands and then using a similar approach to the single island case to find the input variables for each node, using the closest island as a reference from which to calculate z, h and η. Refer to the Appendix for further details of the MATLAB script. From this, an input data file is created for each simulation specifying the initial boundary conditions for each node in the domain.

3.3.2. Tecplot visualisations and analysis

Having obtained the input conditions, the data input files are read and processed to simulate the propagation of the solitary wave and the impact on run-up. For this project, the Tecplot software is used to visualise the wave behaviour over time and to analyse the location and value of the maximum run-up predicted for each island. Tecplot also effectively illustrates wave effects such as reflected waves and the shadow effect as previously described in Section 2.2, and shall be clearly demonstrated in later results. After analysing the output data for maximum run-up height from initial simulations, additional simulations are run at smaller intervals of island spacing, S, and island rotation, θ, where the values obtained vary significantly with noticeable discrepancies.

4. VERIFICATION OF MODEL

4.1. Model setup

For the purpose of verifying the accuracy of the numerical shallow-water Boussinesq-type model, the propagation of the solitary wave and its effect on a single conical island is simulated, and predicted results compared to the experimental results obtained by *Liu et al. (1995)*. In the laboratory experiment, the single island was centred at the local coordinates of X = 12.96m and Y = 13.80m in a wave basin with dimensions of 30m × 25m. Wave gauges were positioned at different locations in the experimental setup; four of which were in front of the island, facing the incident wave, and the other four located around the island. The experimental and numerical results of eight of the gauges are compared to verify the accuracy of the model. The locations of these gauges in the laboratory experiment are defined in *Figure 4* and *Table 1*.

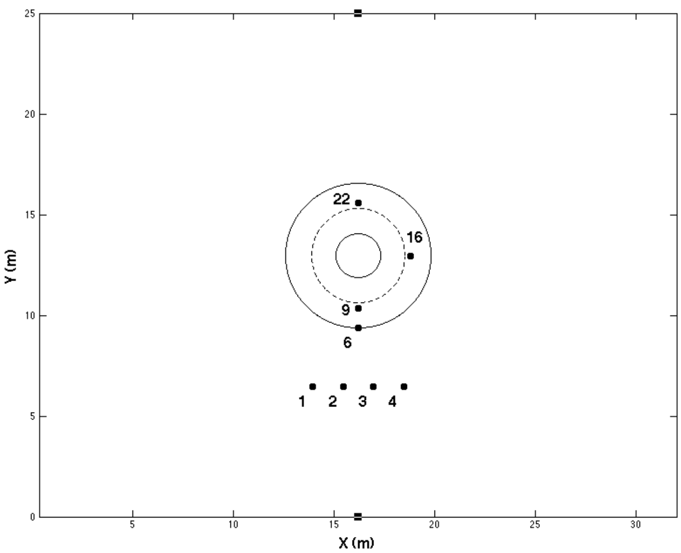

Fig. 4 Schematic of wave gauges in experimental domain

Gauge No.	*X (m)*	*Y (m)*
1	13.95	6.48
2	15.45	6.48
3	16.95	6.48
4	18.45	6.48
6	16.2	9.36
9	16.2	10.36
16	18.78	12.96
22	16.2	15.56

Table 1 Co-ordinates of wave gauges

Simulation of the single-island case required transforming the positions of the wave gauges from the experimental locations to the expanded computational domain, using the centre of the island at the centre of each domain as a reference point. The new positions in the expanded domain are therefore defined in *Figure 5* and *Table 2*.

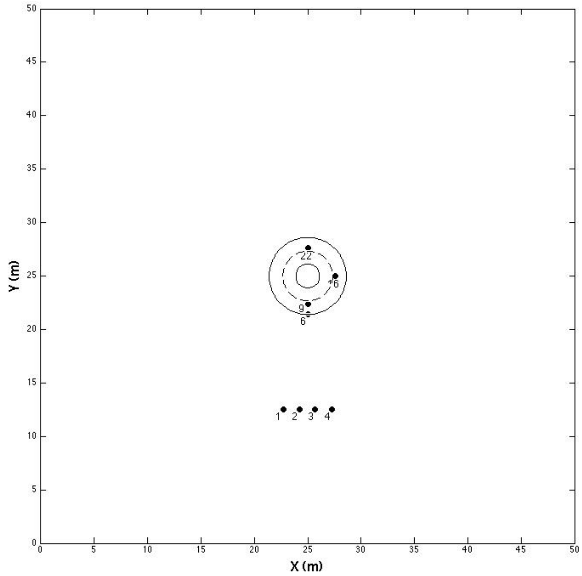

Fig. 5 Schematic of wave gauges in computational domain

Gauge No.	X (m)	Y (m)	i	j
1	22.75	12.5	456	251
2	24.25	12.5	486	251
3	25.70	12.5	515	251
4	27.30	12.5	547	251
6	25.00	21.4	501	429
9	25.00	22.4	501	449
16	27.58	25.0	553	501
22	25.00	27.6	501	553

Table 2 Co-ordinates of wave gauges in expanded computational domain

The co-ordinates of the wave gauges are entered into the simulation as observation points and simulated time histories of the free surface elevations, η, caused by the propagating solitary wave, are predicted.

4.2. Model results

The predicted numerical results are compared with the experimental data obtained from the laboratory experiment of *Liu et al. (1995)*, giving the results in *Fig. 6*. In general, there is a good agreement between the numerical predictions and the experimental data obtained, demonstrating that the propagation of the solitary wave and the moving boundary of the shoreline edge are modelled accurately in the computational simulation.

Gauges 1 to 4 (*Fig. 6(a) – (d)*) are similar in their positions in the computational domain (see *Fig. 5*), located in front of the island, facing the propagating wave, and therefore have similar responses for the free surface elevations. At these gauges, the amplitude of the main wave is modelled extremely precisely, with almost identical values for maximum surface elevation of an average of 0.030645m. Discrepancies in the results occur after the main wave has passed with the numerical results predicting higher surface elevations on average than *Liu et al. (1995)*'s experimental results. It is evident that the numerical results achieve a greater variation in surface elevations above the height of the still water level and the experimental results exhibit a greater variation below the still water level. In addition to this, the slight dip in the water surface level observed at approximately 20 seconds, confirms the reflective behaviour of the incident wave caused by the island.

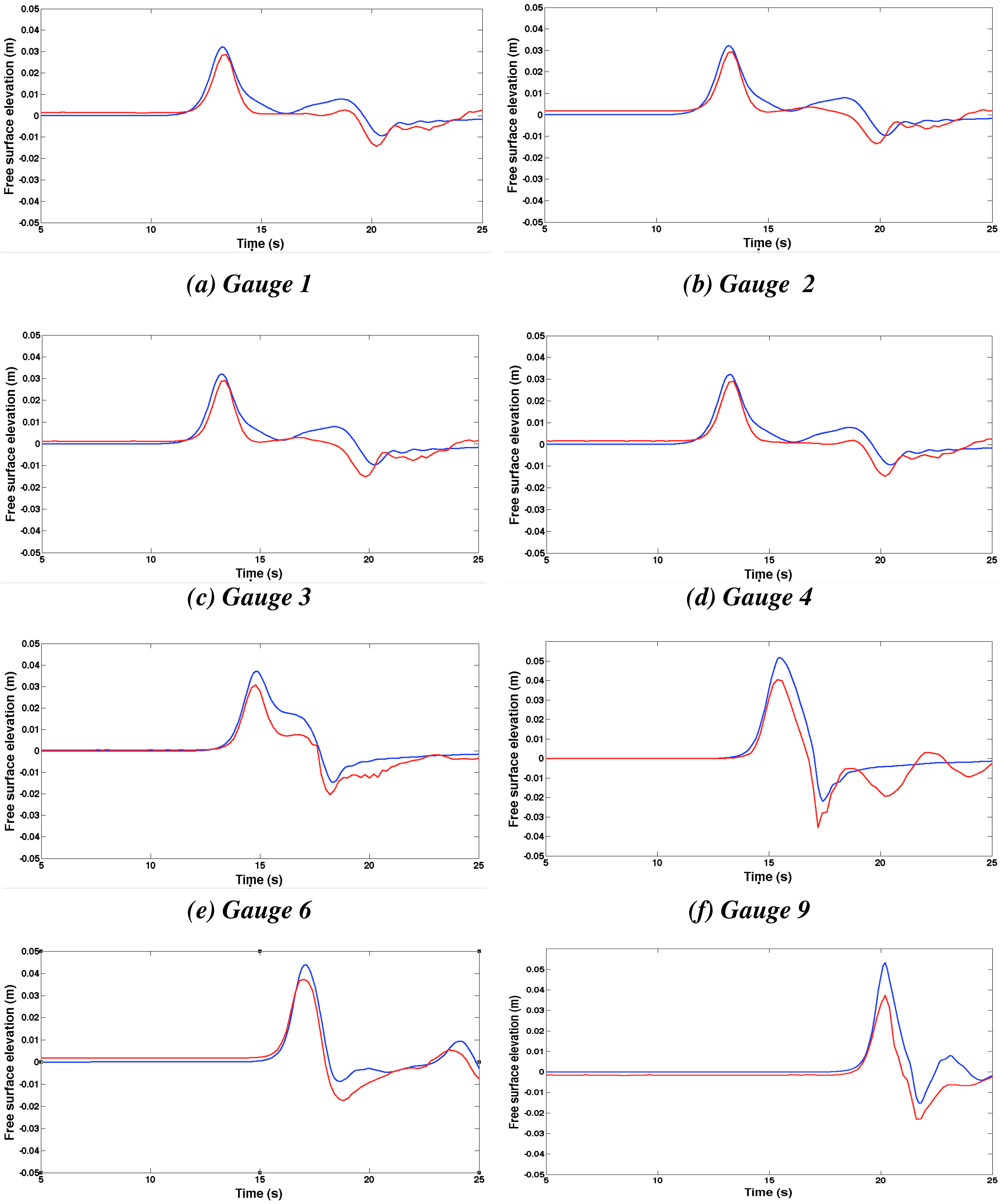

(a) Gauge 1

(b) Gauge 2

(c) Gauge 3

(d) Gauge 4

(e) Gauge 6

(f) Gauge 9

(g) Gauge 16

(h) Gauge 22

Fig. 6 Experimental (red line) and predicted numerical (blue line) time series of free surface elevations at wave gauges 1, 2, 3, 4, 6, 9, 16 and 22

Gauge 6 (*Fig. 6(e)*) demonstrates a good correlation between the experimental and numerical results with both sets of results displaying a similar response. As the gauge is located in front of the island, just above the toe of the island base, the response observed has a greater range than that of Gauges 1 to 4. The numerical prediction of the crest of 0.03713m is also significantly higher than the experimental result of 0.03068m and instead of the response attempting to return to the still water level following the peak, the response for Gauge 6 exhibits a short plateau effect, which may be accounted for by the swash zone effect, in which the water recedes after running a short distance up the slope, contributing to the sustained level of free surface elevation. Subsequently, the water continues to reduce to reach the original still water level.

The response shapes of the numerical predictions and the experimental results of Gauge 9 (*Fig. 6(f)*) generally have good agreement in terms of the occurrence of the amplitude and the immediate response after, which reduces rapidly to a considerably lower level than the initial still water level. However, similar to the other gauges' responses, the numerical prediction of 0.05204m overestimates the amplitude relative to the data obtained through experimental analysis of 0.04048m. After the passing of the main wave, the experimental data exhibits a more oscillatory profile with a greater range of surface elevations, taking longer to return to the original still water level. As Gauge 9 is positioned in front of the island, at the still water level, and facing the propagating wave, this location is likely to experience severe fluctuations in free surface displacement due to the swash zone effect. The variations may be accounted for by the consequential motion of water in the island's swash zone as the water recedes and a secondary layer of water comes in after the wave breaks. This effect has not been fully integrated into the moving boundary's wetting and drying technique, as outlined in Section 3.2, resulting in slight imprecisions in the numerical results.

Gauge 16 (*Fig. 6(g)*), located on the side of the island at still water level (*Fig. 5*), also demonstrates a good agreement between both sets of results. In addition to the higher numerical prediction of the wave amplitude, the response of Gauge 16 also exhibits an underestimation of the extent of the minimum water level, giving a value of almost 0.01m lower for the experimental results than numerical results.

Gauge 22 (*Fig. 6(h)*), located on the lee side of the island at the still water level, experiences extremely high free surface elevations due to the two edge waves wrapping around the island and meeting at this location. Both responses strongly agree but have slight discrepancies in the correlations.

From this analysis of the responses of the eight gauges, it is evident that the model tends to overestimate the surface elevations compared to the experimental results. However, this is considered acceptable, particularly as it gives a conservative prediction for the purpose of determining the safest and most suitable level for construction in coastal regions. Another important feature to note is the smoother response of the free-surface displacement for the numerical results compared to the experimental data. This may be attributed to the expanded computational domain that is incorporated to eliminate the reflective boundary effects, resulting in fewer fluctuations in the numerical data. No boundary reflected waves are encountered in the numerical simulation so no disturbance is caused to the predicted run-up heights, therefore validating the model.

The interaction between the propagating solitary wave and the isolated single island is clearly characterised in the snapshots of *Figure 7*, which illustrate the high run-up experienced on the front of the island (*Fig. 7(a)*), with the formation of edge waves wrapping around and colliding, generating high run-up on the lee side (*Fig. 7(c)*).

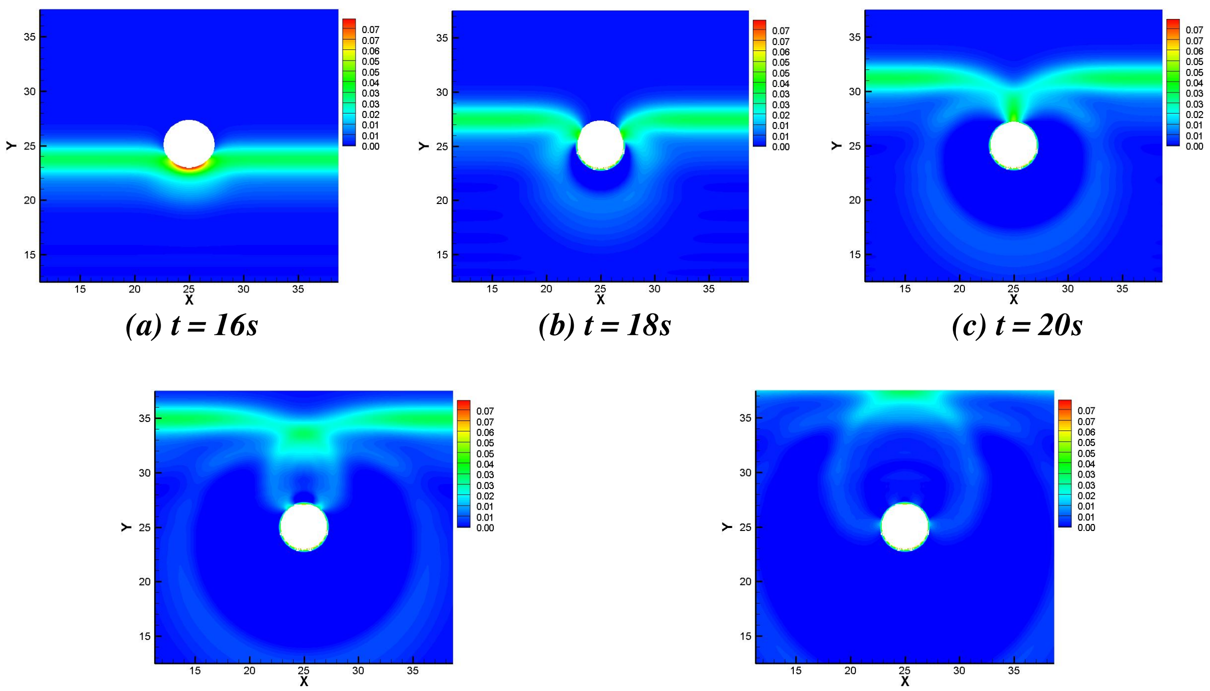

(a) t = 16s ***(b) t = 18s*** ***(c) t = 20s***

(d) t = 22s ***(e) t = 24s***

Fig. 7 Interaction between propagating solitary wave and isolated single island

The numerical model is further verified using a comparison of the maximum run-up heights recorded at various locations around the perimeter of the island, as demonstrated in *Figures 8* and *9*.

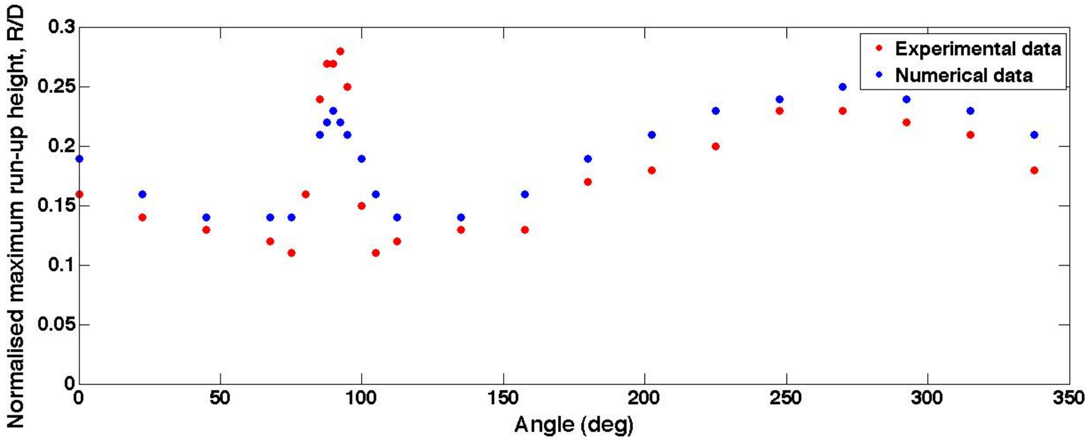

Fig. 8 Comparison of Liu et. al (1995)'s experimental and predicted numerical run-up heights normalised with the still water depth, D=0.32m, and angle as defined in Fig. 9

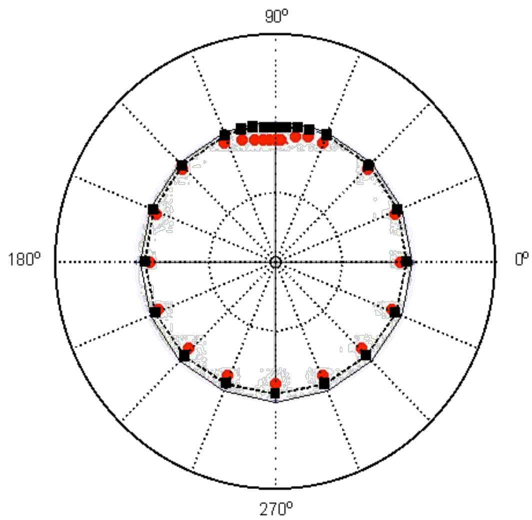

Fig. 9 Polar plot of experimental (black dots) and numerical (red dots) maximum run-up

Figure 8 demonstrates a fairly strong agreement in the maximum run-up heights recorded around the perimeter of the island. As expected, the front of the island facing the incident wave experiences a significantly high run-up height of 7.928cm measured numerically at θ = 270°. The narrow wake on the lee side of the island also experiences a notably high run-up due to the interaction between the two edge waves as they meet, giving a numerical value of 7.352cm measured at θ = 90°. The two distinct narrow bands of particularly low surface elevation on the island's lee side represent the sheltered regions, bounded by lines of angles of 10° and 30° on either side of the island's centreline (θ = 90°), as concluded by *Liang, Borthwick and Romer-Lee, 2012*. Generally, the numerical model provides an overestimate of run-up height, however, on the lee side of the island (θ = 90°), the experimental results were found to exceed the numerical predictions by up to 0.016m. The polar plot of *Figure 9* shows a notable match between the computed numerical and observed run-up heights around the island, with the numerical model giving slightly more conservative results with regards to the location of the maximum run-up. Despite the discrepancies, in general, the results have a strong agreement, verifying the accuracy of the numerical model. It is therefore deemed reliable in demonstrating the impact of a solitary tsunami wave, and can hence be used for simulating the three-island cluster scenarios.

5. APPLICATION OF NUMERICAL MODEL TO THREE-ISLAND CASE

5.1. General observations of response

For the case of the three-island cluster, the numerical model for solving the shallow-water Boussinesq-type equations is again used to investigate the propagation of a solitary wave, and its interaction with varying arrangements of three islands. As outlined in Section 3.3.1, the centre of the cluster is located at the centre of the computational domain (X = 25, Y = 25m), and the parameters, S and θ, are to vary, where S is the island separation, and θ is the angle of rotation of Island 1 relative to the direction of the incident wave as defined in *Figure 3*. The centre-to-centre island separation, S, is non-dimensioned using the island diameter at still water level, d = 4.64m, to form the parameter S/d. This varies from 1, corresponding to the case of merged islands at the still water level, to 3, corresponding to the case of completely separated islands. The intermediary values of 1.25 and 1.5 correspond to the case of merged islands below the still water level. The angle of rotation, θ, varies from 0° to 60° to avoid repetition in the analysis, as explained previously, initially in intervals of 15°, then with additional simulations run at θ = 5°. Initial conditions are generated and simulations run for different combinations of island spacing and rotation using MATLAB and TecPlot, and the maximum run-up heights and corresponding locations are analysed for each island.

Figures 10(a) – (c) demonstrate the variability in maximum run-up heights predicted numerically for each island. These results are illustrated in 3D surface plots in *Figures 11(a) – (c)* to enable a clearer visualisation of the variability in run-up heights.

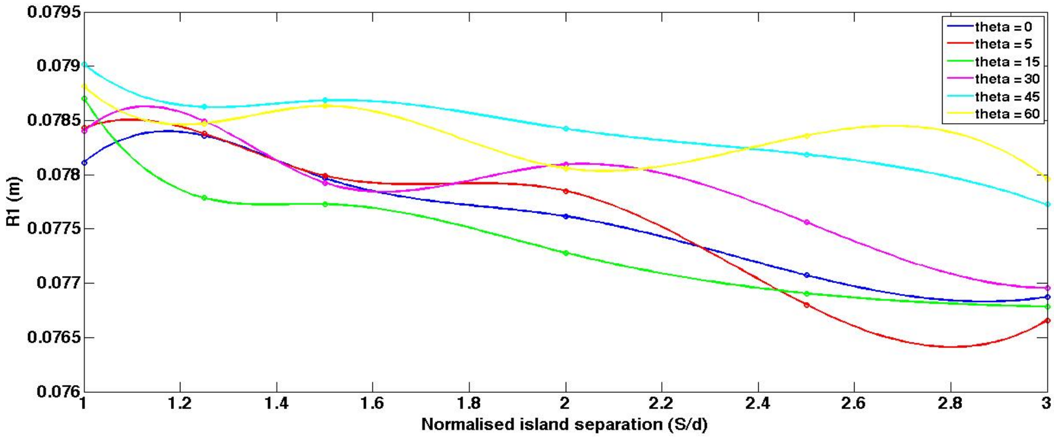

(a) Variation in maximum run-up height, R1, on Island 1

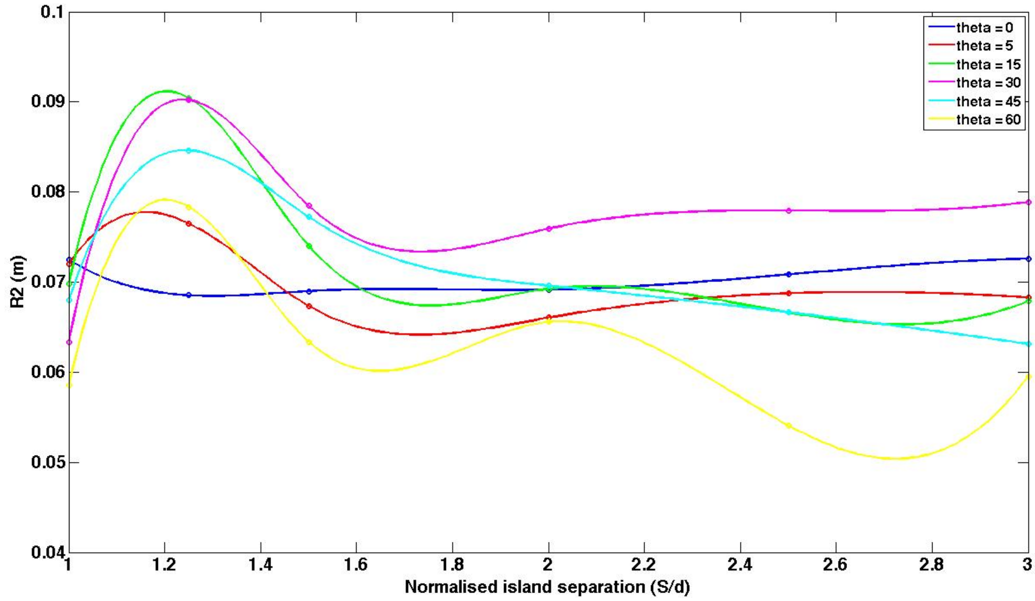

(b) Variation in maximum run-up height, R2, on Island 2

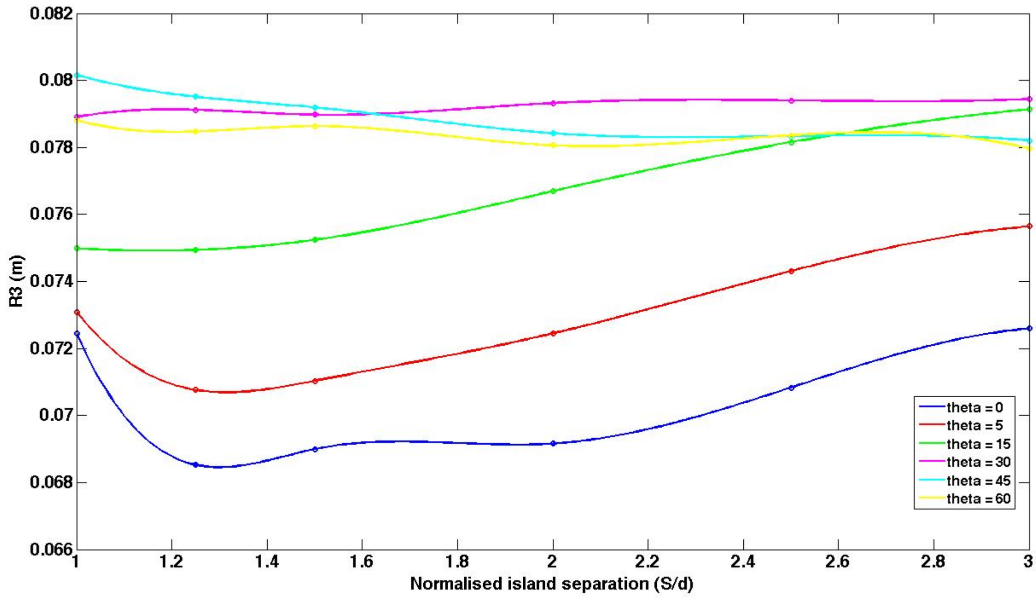

(c) Variation in maximum run-up height, R3, on Island 3

Fig. 10 Numerical predictions of maximum run-up heights

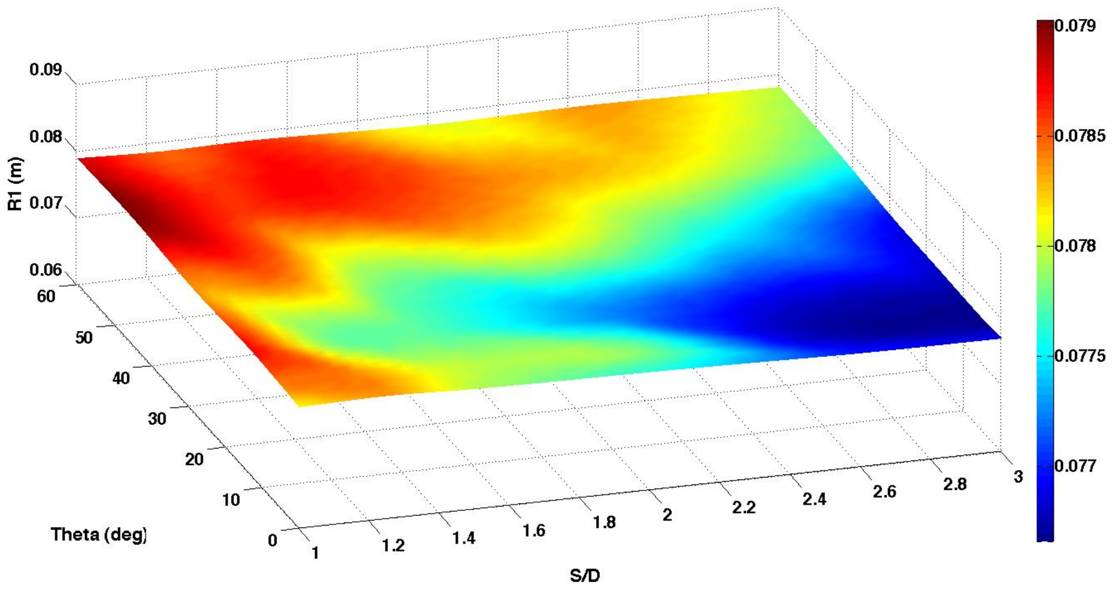

(a) Surface plot of maximum run-up height, R1, on Island 1

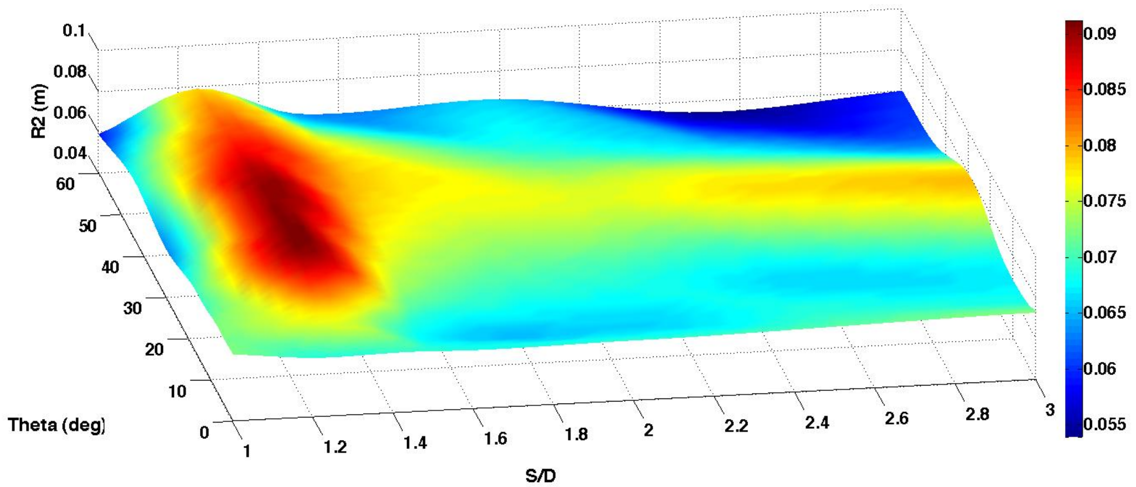

(b) Surface plot of maximum run-up height, R2, on Island 2

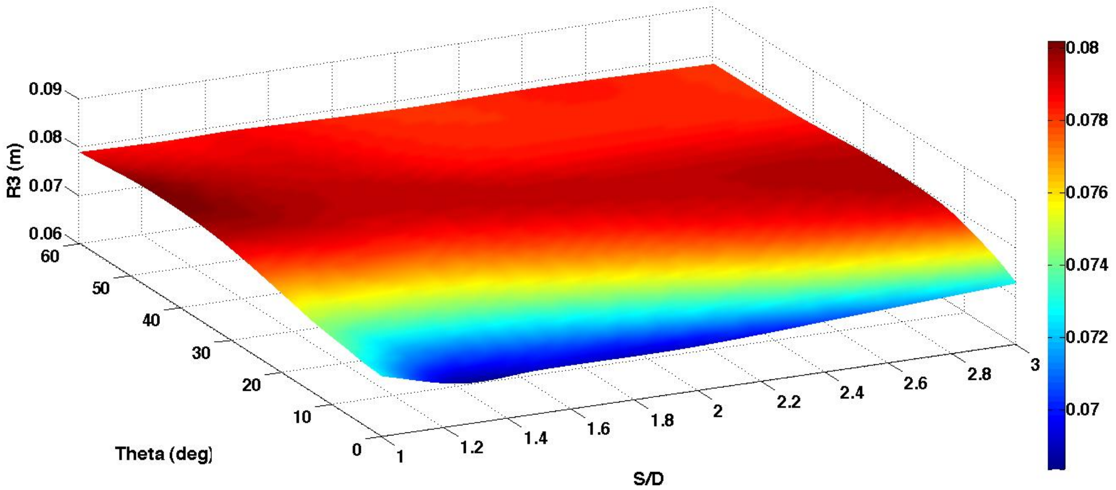

(c) Surface plot of maximum run-up height, R3, on Island 3

Fig. 11 3D surface plots of maximum run-up heights

Figures 10 and *11* exhibit some noticeable patterns of behaviour with regards to the numerically predicted maximum wave run-up heights. As the island separation, S/d, increases, it is expected, in general, that the maximum run-up on Island 1, R1, decreases due to a reduction in the level of interference caused by reflected waves from the other two islands. As the islands are located further apart, there is a gradual transition in the behaviour of the wave as the islands become more representative of separate single islands. In general, this response is observed for most of the angles. There are, however, a few discrepancies at $\theta = 0°$ and at the higher angles of $\theta = 30°$, $45°$ and $60°$ for smaller separations of 1.25 and 1.5, where the responses are observed to increase slightly before descending.

As θ increases, a rise in R1 is expected due to the reflective behaviour of Island 2 as it moves behind Island 1. At small separations, this behaviour is observed, however, as S/d increases, the effect decreases as Island 2 becomes more distant and provides a less effective reflective boundary. Observations and discrepancies are discussed in further detail later by examining the locations of maximum predicted run-up heights.

Figure 10(b) suggests that the predicted run-up on Island 2 is consistently lower than that of the other islands with a significantly smaller range. This is accounted for by the shadow effect provided either partially or fully by the two upstream islands. Analysis of Island 2 suggests that as island separation increases, the maximum wave run-up height on Island 2, R2, decreases after a critical value of S/d is reached. Before this critical value of approximately $S/d \approx 1.25–1.5$, at which, the islands are considered to be partially merged below the still water level, R2 increases due to the interaction effect of the combined edge waves of Island 1 meeting on the lee side in close proximity to Island 2. At the critical value of S/d, R2 is observed to reach its maximum value, before decreasing as S/d exceeds this value. At this point, the energy of the wave has been dissipated at Island 1 and there is less interference from the nearby edge waves of Island 1. This is the general behaviour observed, however, a significant discrepancy occurs at $\theta = 30°$, where R2 is seen to increase beyond a separation of $S/d = 2$. Another key observation is the significantly low value of R2 at a separation of $S/d = 3$ and at $\theta = 60°$. These effects are investigated in greater detail in Section 5.2.

As θ increases, an increase in R2 is also observed, with this behaviour being most significant at a separation of $S/d = 1.25$. Generally, this occurs up until a value of $\theta = 30°$, which is representative of the case of Island 2 being located directly behind Island 1. This effect is also considered in more detail in the next section. It is important to note that at a low separation of S/d = 1, the R2 profile exhibits slightly different behaviour. As θ increases, R2 decreases until the critical point of $\theta = 30°$ when Island 2 is in the shadow of Island 1. It is evident that Island 2 has the most interesting and unusual response to the impact of the propagating wave, and therefore requires much further detailed examination and analysis on the locations of the predicted results around the island. It is, however, expected that as Island 2 moves into the sheltered region of Island 1, the location of R2 should shift along the upstream face of the island towards the centre line of the domain, as concluded by *Chen and Liang (2012)* in a study on two-island clusters.

In general, the maximum run-up on Island 3 is observed to increase with θ. The profile R3, however, presents little variation with island separation, S/d, for $\theta \geq 30°$. Above this critical angle, Island 3 has very little interaction with the other islands and begins to move to be in line with Island 1, therefore taking the impact of the incident wave more directly, resulting in high values of R3. Below $\theta = 30°$, however, R3 decreases as island separation increases. The rate at which this occurs is also found to be dependent on separation. At small separations, typically for values of S/d = 1–1.5, at which the islands are merged either at or below the still water level, the value of R3 tends to decrease at a slower rate than for values of S/d ≥ 1.5, at which the islands are completely separated. Another significant effect to be noted is the decrease in run-up, R3, as separation increases, for the case of $\theta = 45°$, which shall also be examined in more depth.

5.2 Detailed analysis of numerical observations

The detailed analysis of the numerical simulations is divided into three classifications; the case of islands merged at still water level (i.e. S/d = 1), the case of islands merged below still water level (i.e. 1 ≤ S/d ≤ 1.55), and the case of separated islands (i.e. S/d ≥ 1.55), each of which shall be addressed individually.

5.2.1 Islands merged at still water level (S/d = 1)

At an island separation of S/d = 1, the islands are merged at still water level, resulting in a narrow channel between the islands, in which a large run-up can accumulate. *Figure 12* shows the variation in the maximum run-up with θ.

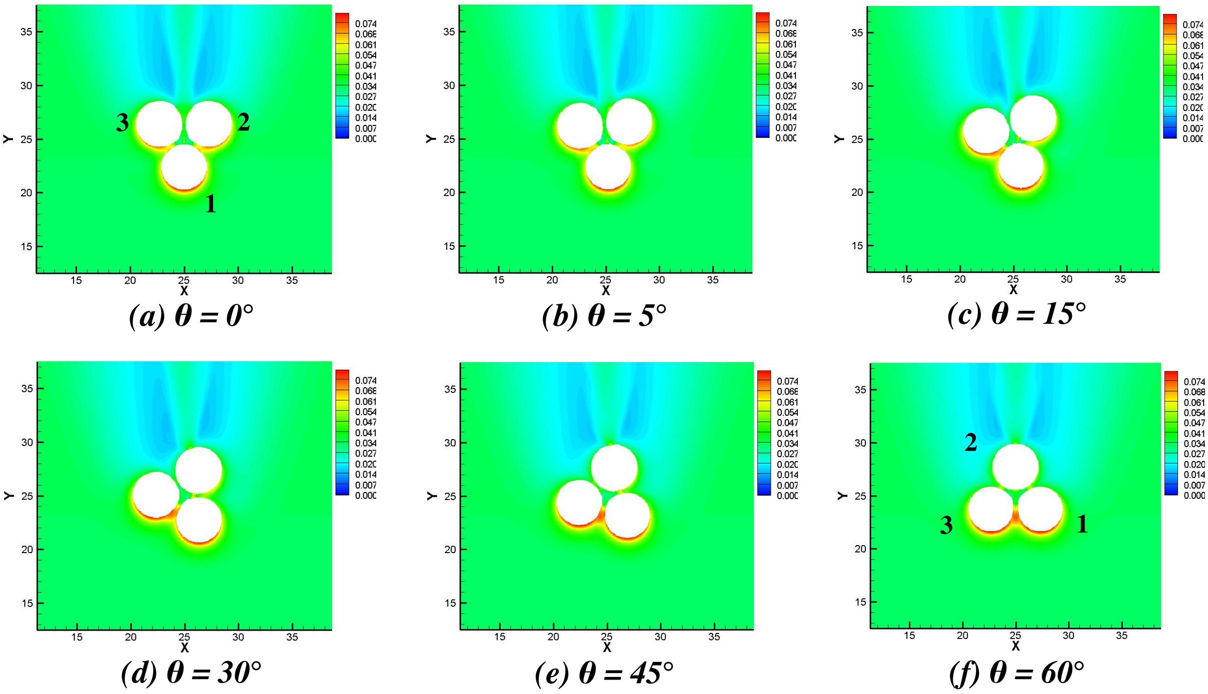

(a) θ = 0° *(b) θ = 5°* *(c) θ = 15°*

(d) θ = 30° *(e) θ = 45°* *(f) θ = 60°*

Fig. 12 Maximum run-up for merged islands (S/d = 1)

It is evident that as θ increases, the maximum run-up on Island 2 reduces from 0.0725m at θ = 0° to 0.0586m at θ = 60° as it moves into the shadowed regions of Islands 1 and 3, which rotate to increase the bearing width of the island cluster, taking the impact of the incident wave more directly. As expected, a wake is produced on the lee side of the island cluster with a high surface elevation and narrow bands of sheltered regions on either side. It is important to note that at such a low separation, the islands effectively act as a single entity, producing one wake. At higher angles of 30° (*Fig. 12(d)*), 45° (*Fig. 12(e)*), and 60° (*Fig. 12(f)*), a high surface elevation is recorded in the narrow channel between Islands 1 and 3 as they become aligned perpendicular to the direction of the incident wave. From *Figure 12* it is noticeable that the maximum run-up of Island 1, R1, consistently occurs at the front of the island as θ increases, and that of Island 3, R3, also occurs at the front of the island, slightly off the centre line for 0° ≤ θ ≤ 15° due to the shadow effect of Island 1, but shifts towards the centreline for θ ≥ 15° as it becomes increasingly exposed to the propagating wave. The locations of the maximum run-up on Island 2, R2, however, are much more unpredictable, as illustrated in *Figure 13*, and require further analysis.

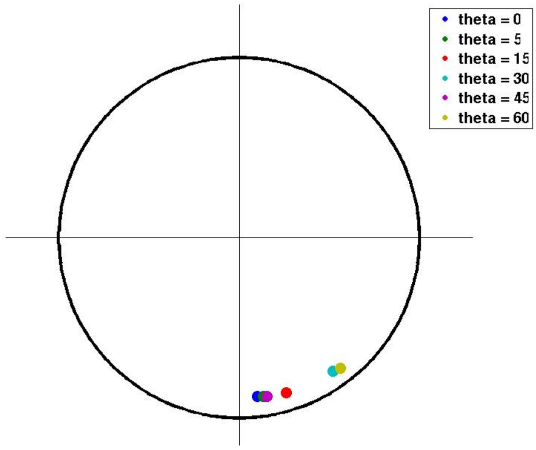

Fig. 13 Locations of maximum run-up, R2, for S/d = 1

The location of R2 is generally found to move in one direction around the island, to the regions that remain exposed to the direct impact of the wave, as the island begins to move into the sheltered region of Island 1. There is, however, one discrepancy in the location of R2 at θ = 45°. At this angle, Island 2 is entirely in the shadow of the other two islands, and is no longer exposed to the direct impact of the wave.

The interaction between the propagating solitary wave and the merged three-island cluster at θ = 30° is clearly characterised in the snapshots of *Figure 14*.

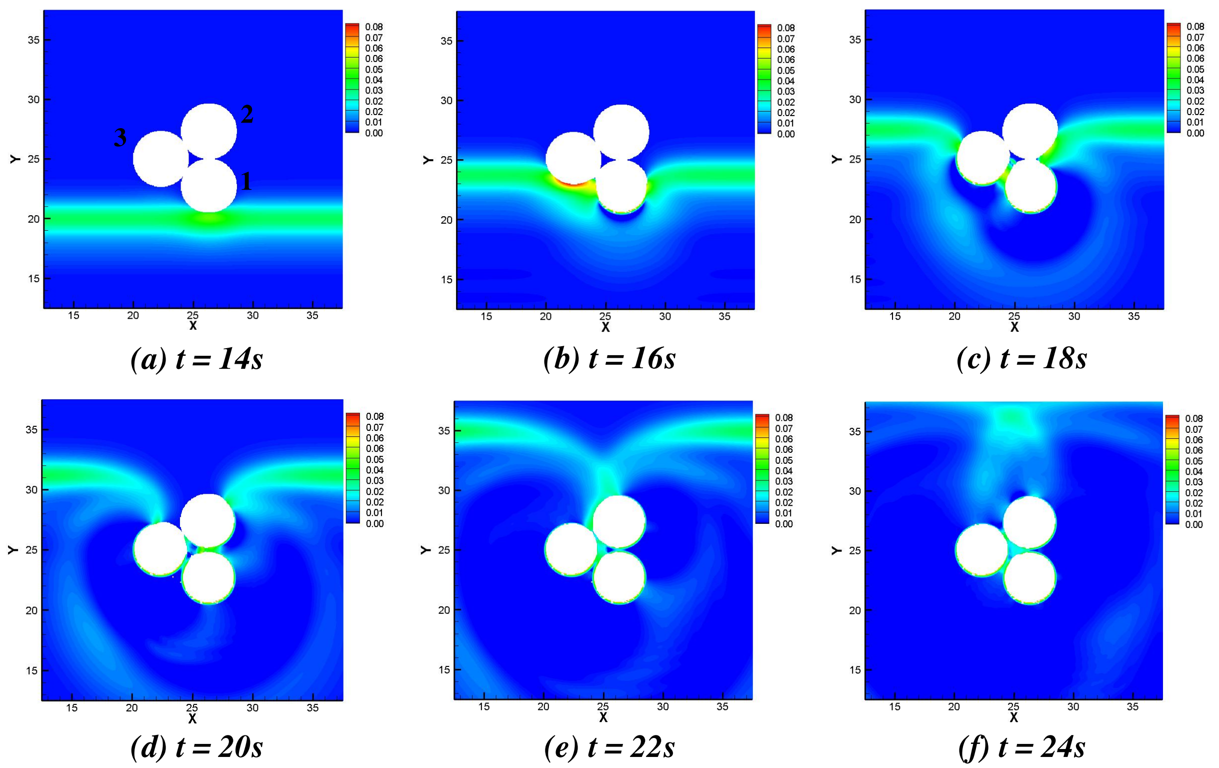

(a) t = 14s *(b) t = 16s* *(c) t = 18s*

(d) t = 20s *(e) t = 22s* *(f) t = 24s*

Fig. 14 Interaction between propagating solitary wave and merged triple-island cluster (S/d = 1, θ = 30°)

As Island 3 is almost completely exposed directly to the impact of the wave, a high run-up is recorded on the front of this island of 0.0789m, slightly lower than that recorded for a single island of 0.0793m. The reflected wave produced by the incident wave acting on Island 3 merges with the larger reflected wave produced by Island 1 (*Fig. 14(c))*, which soon becomes distorted (*Fig. 14(d)*). As described previously, large run-ups are recorded in the narrow channels between the islands, particularly between Islands 1 and 3. A single wake is observed on the lee side of Island 2 (*Fig. 14(e)*) owing to the island cluster behaving as a single entity.

5.2.2 Islands merged below still water level (1 ≤ S/d ≤ 1.55)

For islands that are partially merged below the still water level, the channel between the islands is widened, allowing a greater flow of water to continue to propagate downstream. *Figures 15* and *16* illustrate the variation in maximum run-up for the two simulated cases: S/d = 1.25 and S/d = 1.5.

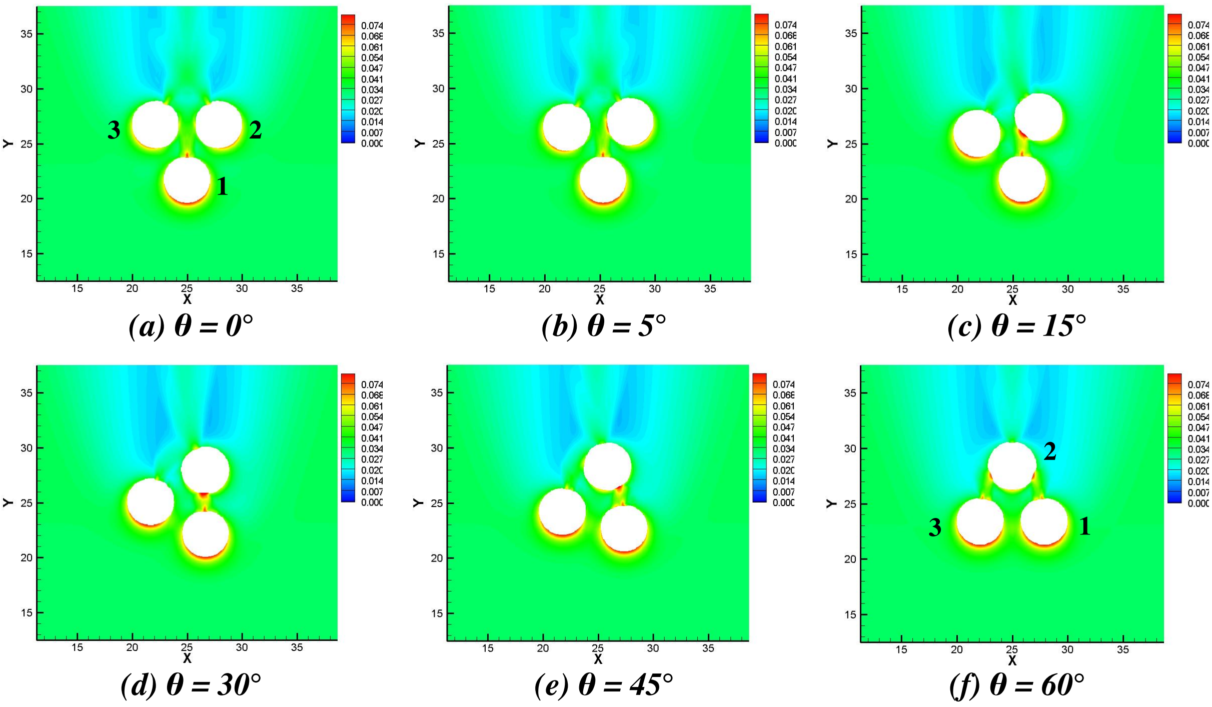

(a) θ = 0° ***(b) θ = 5°*** ***(c) θ = 15°***

(d) θ = 30° ***(e) θ = 45°*** ***(f) θ = 60°***

Fig. 15 Maximum run-up for partially merged islands (S/d = 1.25)

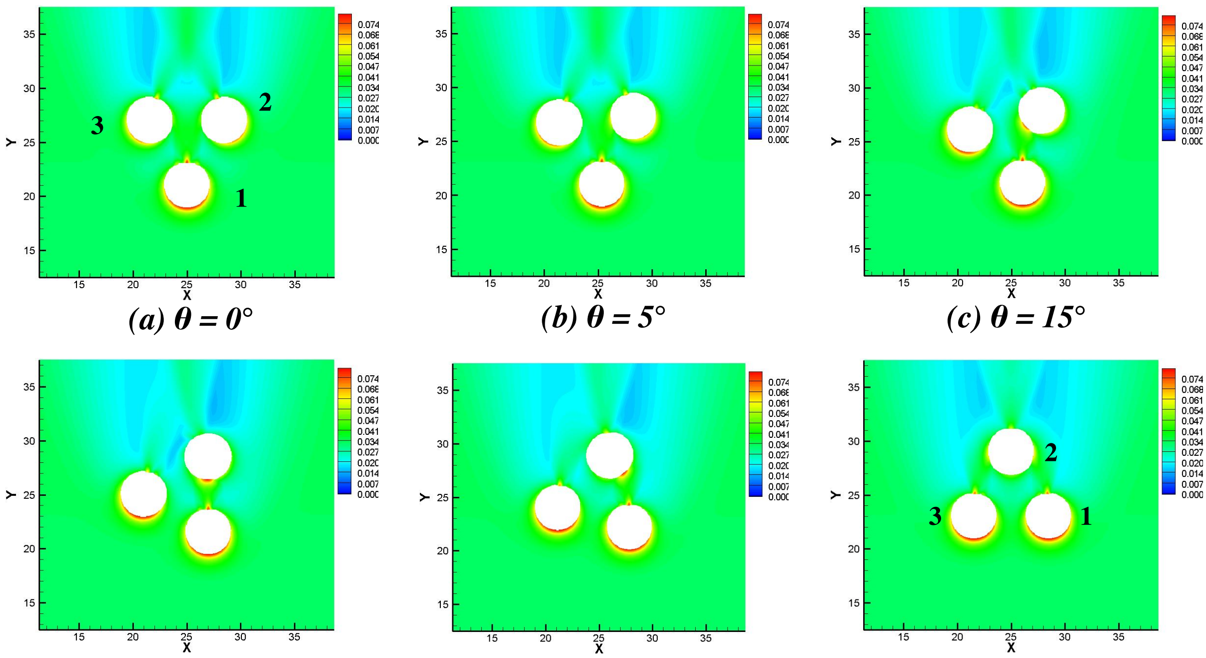

(a) $\theta = 0°$ (b) $\theta = 5°$ (c) $\theta = 15°$

(d) $\theta = 30°$ (e) $\theta = 45°$ (f) $\theta = 60°$

Fig. 16 Maximum run-up for partially merged islands (S/d = 1.5)

In the case of partially merged islands, joined below still water level, the islands begin to exhibit similar behaviour to that of separated islands, with small wakes forming on the lee side of the downstream islands. This is due to the increased separation allowing an expanded channel of water to flow between the islands to continue the propagation of the wave, and to wrap around the islands as edge waves, meeting at the rear to form higher levels of surface elevation. The islands are, however, insufficiently separated to avoid interference between the two individual wakes. *Figures 15* and *16* demonstrate the wake of Islands 2 and 3 and the inner bands of the sheltered regions coinciding. This is partly due to the direction of the wakes induced, which are not oriented parallel to the incident wave, and therefore result in interference. As described in Section 5.1, as θ increases, the maximum run-up on Island 2, R2, for S/d = 1.25, increases from 0.0685m at θ = 0° to 0.0902m at θ = 30°, the point at which Island 2 lies directly in the shadow of Island 1. This is accounted for by the joining edge waves of Island 1 interacting with Island 2 at such close proximity, and the narrow channel that exists between the islands. At a larger separation of S/d = 1.5, the run-up, R2, is observed to be slightly lower than that of S/d = 1.25, increasing from 0.0690m at θ = 0° to 0.0784m at θ = 30°, owing to the wider channel reducing the interaction effect between the wave and Island 2.

Comparable to the merged islands at still water level considered in Section 5.2.1, R1 consistently occurs at the front of Island 1, and R3 is observed to occur primarily on the upstream side of Island 3, shifting towards the centre-line as θ increases and the island moves out of the sheltered region of Island 1 whilst becoming more exposed to the direct impact of the propagating wave. A discrepancy at a separation of S/d = 1.5 and θ = 0°, however, sees R3 occurring on the downstream side of the island, as it lies protected in the sheltered region of Island 1. The unpredictable locations of R2 are examined in further detail in *Figure 17*.

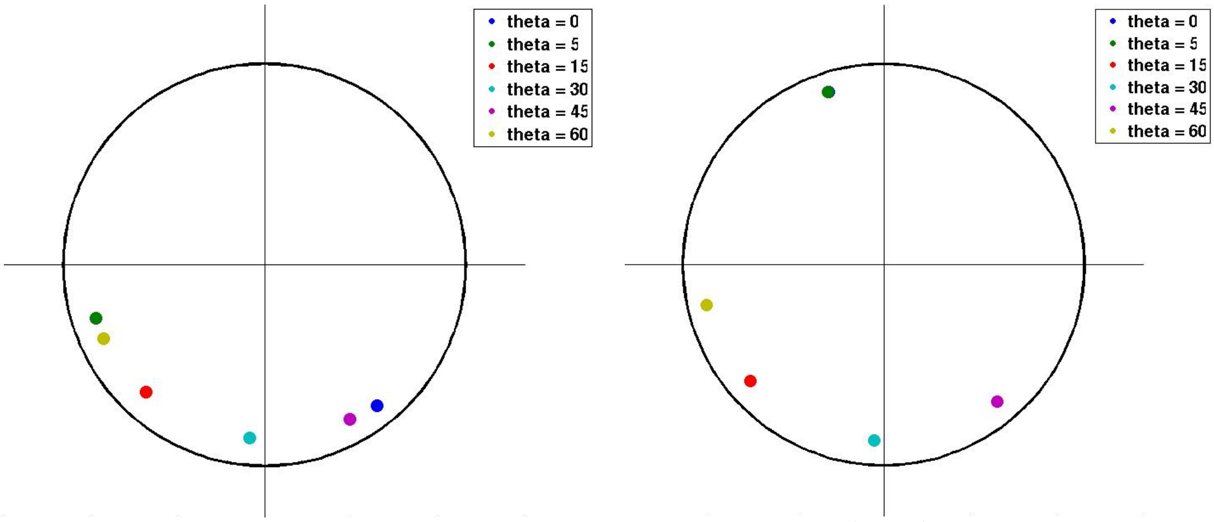

(a) S/d = 1.25 ***(b) S/d = 1.5***

Fig. 17 Locations of maximum run-up, R2

For a separation of S/d = 1.25 (*Fig. 17(a)*), the location of R2 gradually moves along the upstream side of Island 2 as θ increases. These locations correspond to the points directly downstream of the high surface elevations recorded on the lee side of Island 1, as a result of the high flow in the narrow channel between the islands, demonstrated in *Figure 15*. For a separation of S/d = 1.5 (*Fig. 17(b)*), the locations for R2 are found to be similar to those of S/d = 1.25 in the range of 15° ≤ θ ≤ 60°, however, at smaller rotations of θ = 0° and θ = 5°, R2 is located on the downstream side of Island 2. From *Figure 16*, it can be observed that at these angles, no region of Island 2 lies directly downstream of the centre-line of Island 1 and it is therefore not exposed to the direct impact of the wake of Island 1, thus giving reduced values of R2. Instead, at these angles, R2 is induced by the island's own edge waves coinciding on the lee side.

The interaction between the propagating solitary wave and the partially merged three-island clusters with S/d = 1.25 and θ = 15°, and S/d = 1.5 and θ = 45°, is clearly characterised in the snapshots of *Figures 18* and *19*.

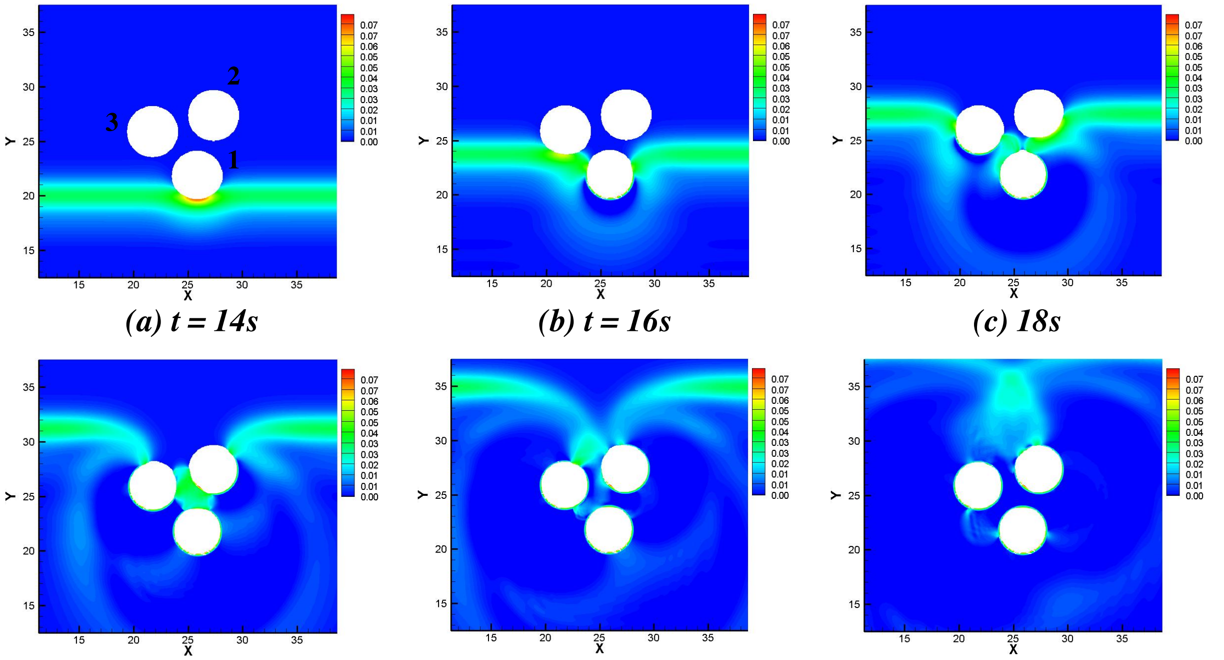

(a) $t = 14s$ (b) $t = 16s$ (c) $18s$

(d) $t = 20s$ (e) $t = 22s$ (f) $t = 24s$

Fig. 18 Interaction between propagating solitary wave and partially merged triple-island cluster ($S/d = 1.25, \theta = 15°$)

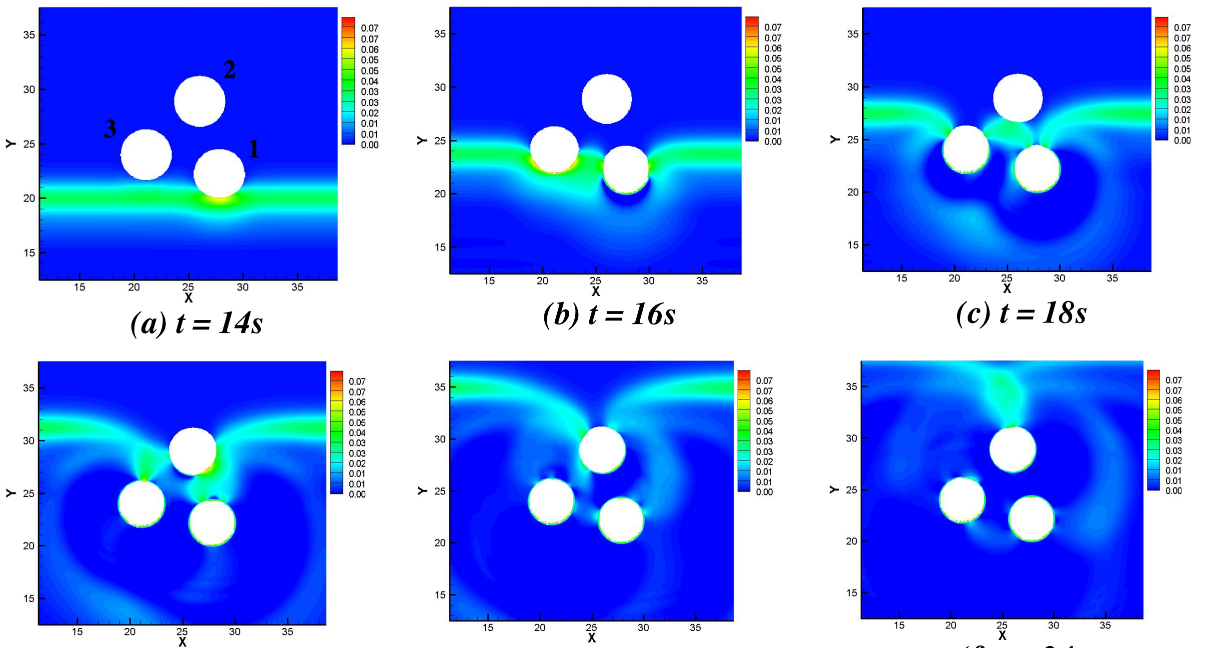

(a) $t = 14s$ (b) $t = 16s$ (c) $t = 18s$

(d) $t = 20s$ (e) $t = 22s$ (f) $t = 24s$

Fig. 19 Interaction between propagating solitary wave and partially merged triple-island cluster ($S/d = 1.5, \theta = 45°$)

The onset of the incident wave produces an extremely high run-up on the upstream side of Island 1 (*Fig. 18(a)* and *Fig. 19(a)*) and Island 3 (*Fig. 18(b)* and *Fig. 19(b)*) as they face the direct impact of the propagating wave; both producing reflected waves in the process. As much of the wave's energy is dissipated at the two upstream islands, a smaller and weaker reflected wave is generated at Island 2. As the wave continues to propagate past Island 2, a large run-up, R2, and high surface elevations are also recorded at the centre of the island cluster (*Fig. 18(d)*). This is due to the refractive, diffractive and shoaling behaviour of the wave as it approaches the narrow channels between the islands. As the separation is sufficiently large to allow the flow of water between the islands, separate wakes are formed for Islands 2 and 3 (*Fig. 18(e)*). At a larger separation of S/d = 1.5, the narrow channel between the islands widens, and the wave begins to continue to propagate past the islands with an observed reduction in the refractive, diffractive and shoaling effects in the centre of the cluster (*Fig. 19(c)* and *(d)*).

5.2.3 Separated islands (S/d ≥ 1.55)

For separated islands, the interaction effect between individual islands is less significant and for large separations, the diffraction and refraction effects are less noticeable. As S/d increases, the region between the islands becomes less representative of a narrow channel, enabling the water to flow more freely and the wave to continue to propagate past the islands. *Figures 20*, *21* and *22* demonstrate the variation in maximum surface elevation for the three cases of separated islands: S/d = 2, 2.5 and 3.

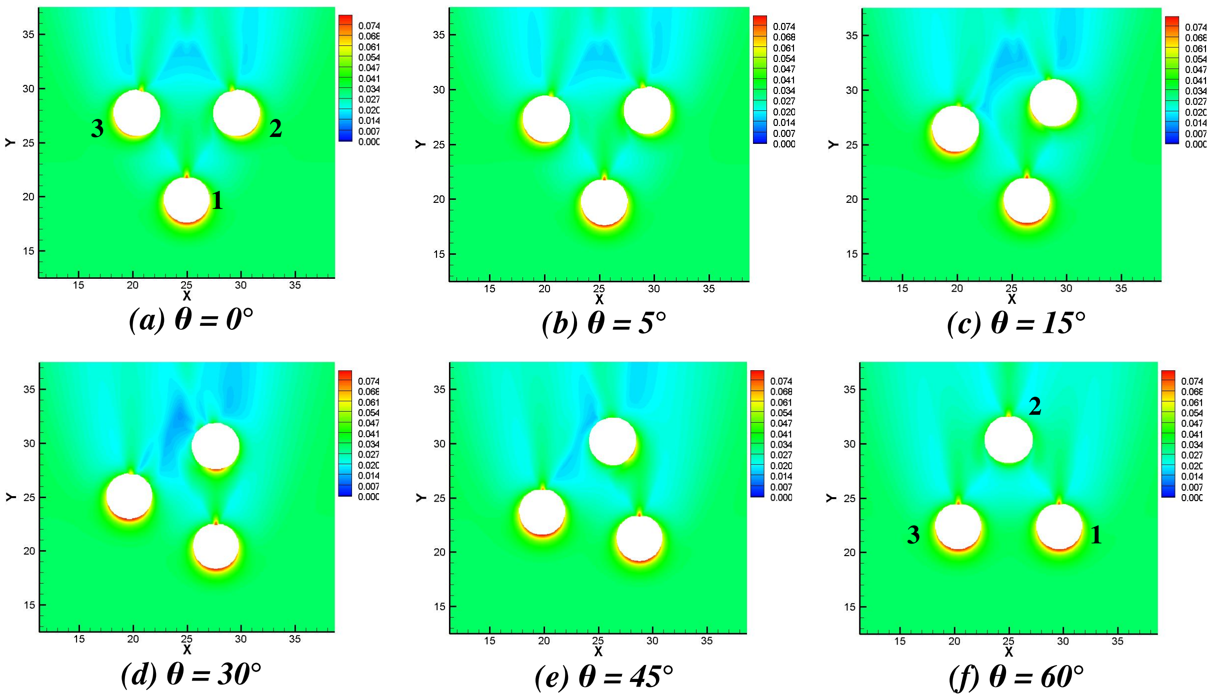

(a) θ = 0° ***(b) θ = 5°*** ***(c) θ = 15°***

(d) θ = 30° ***(e) θ = 45°*** ***(f) θ = 60°***

Fig. 20 Maximum run-up for separated islands (S/d = 2)

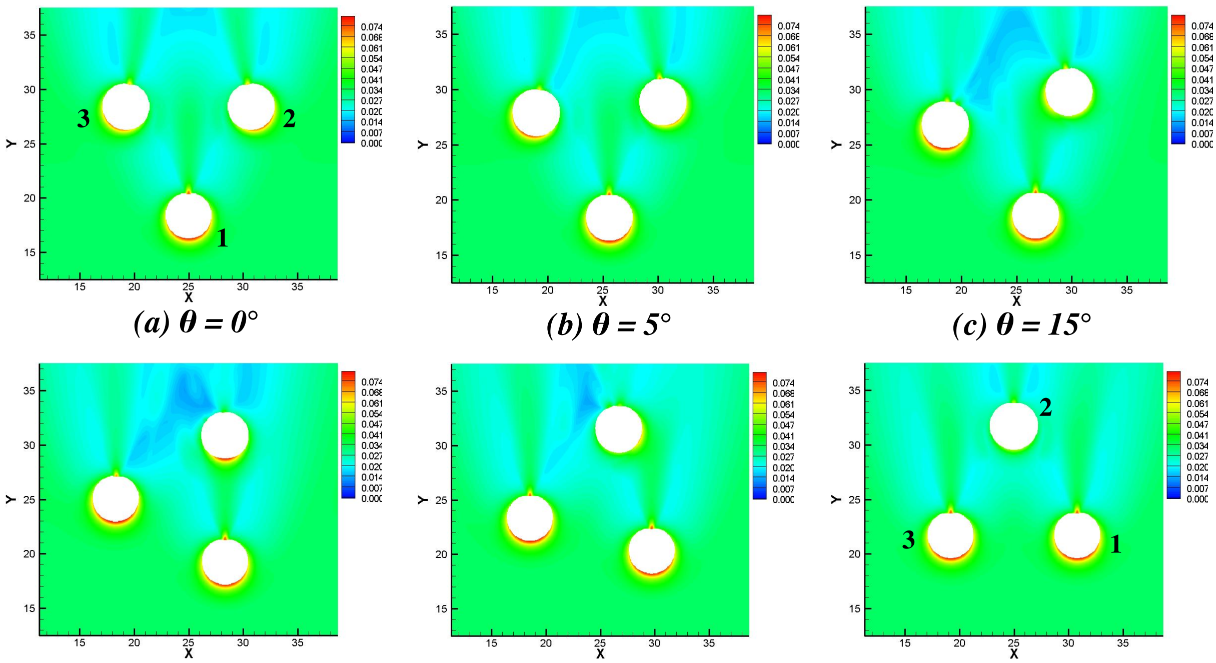

(a) $\theta = 0°$ (b) $\theta = 5°$ (c) $\theta = 15°$

(d) $\theta = 30°$ (e) $\theta = 45°$ (f) $\theta = 60°$

Fig. 21 Maximum run-up for separated islands (S/d = 2.5)

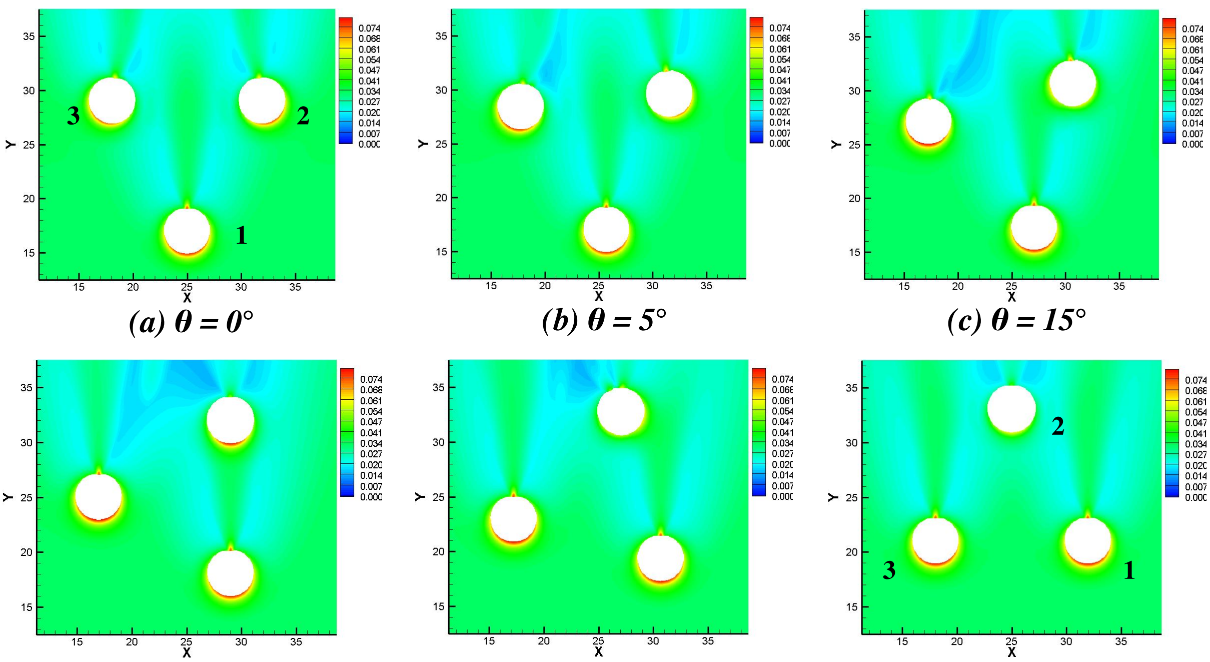

(a) $\theta = 0°$ (b) $\theta = 5°$ (c) $\theta = 15°$

(d) $\theta = 30°$ (e) $\theta = 45°$ (f) $\theta = 60°$

Fig. 22 Maximum run-up for separated islands (S/d = 3)

In the case of fully separated islands, Islands 1 and 3 behave in a similar manner to isolated single islands, both with large run-up on the upstream side and relatively large run-up on the lee side with the formation of a wake and sheltered regions on either side of the wake. Both islands experience very little fluctuation in run-up as the cluster arrangement is rotated.

Island 1 is consistently the furthest island upstream and therefore receives the greatest impact of the propagating wave, resulting in a slightly higher run-up than Island 3 at low angles. As θ increases, Island 3 moves away from the sheltered regions of Island 1 and faces the incident wave directly, generating a larger value of run-up. When the angle of rotation exceeds approximately 30°, however, the orientation of the island cluster has a limited effect on the run-up recorded, and the island effectively acts a single isolated island. This effect is most noticeable at the larger separation of S/d = 3 (*Fig. 22*). While Islands 1 and 3 experience only small fluctuations in run-up, the variation in island separation, S/d, and angle of rotation, θ, still have a considerable influence on the run-up predicted on Island 2, ranging from 0.0541m at S/d = 2.5 and θ = 60°, to 0.0789m at S/d = 3 and θ = 30°. Due to the large wake produced and the shadow effect provided by the two islands upstream, the locations of R2 are still observed to be irregular, as demonstrated by *Figure 23*.

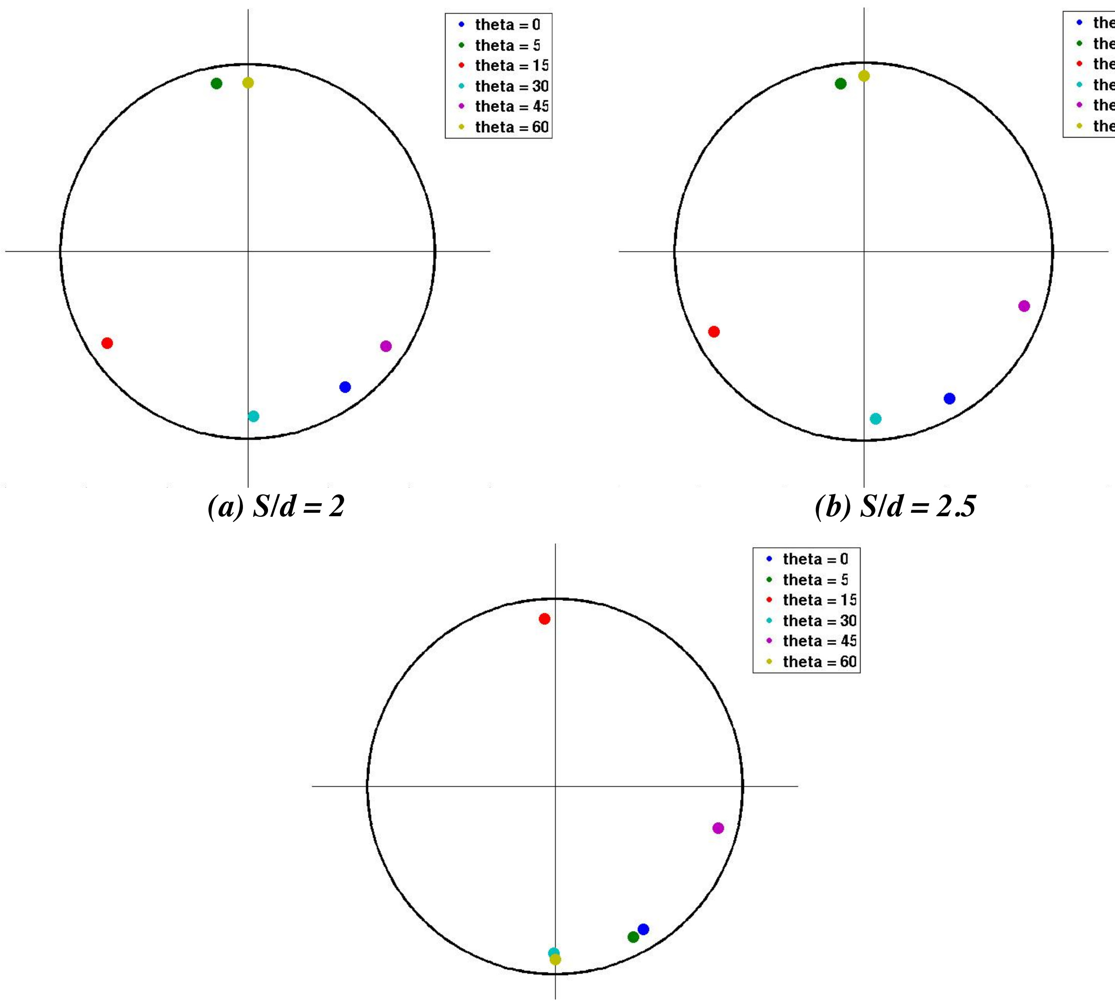

(a) S/d = 2 ***(b) S/d = 2.5***

(c) S/d = 3

Fig. 23 Locations of maximum run-up, R2

At separations of S/d = 2 and S/d = 2.5, R2 is located generally on the upstream half of the island. At $\theta = 0°$, Island 2 is entirely exposed to the propagating wave and R2 occurs at a point clear of the sheltered region of Island 1. In the range $0° \leq \theta \leq 15°$, Island 2 moves into the sheltered region of Island 1, resulting in reduced run-up and the location of R2 on the lee side of the island (*Fig. 23(a)* and *(b)*). As $\theta = 15°$ is approached, the island begins to move out of the sheltered region and into the large wake (*Fig. 20(c), Fig. 21(c)* and *Fig. 22(c)*), shifting the location of R2 again to the upstream half of the island (*Fig. 23(a)* and *(b)*). At $\theta = 30°$, R2 is observed to consistently occur on the centre-line on the front of the island. This is attributed to the long wake of Island 1. For the island separations investigated in this study, i.e. $1 \leq S/d \leq 3$, Island 2 is consistently found to lie in the long wake of Island 1 for this particular angle. However, this may not be the case for larger separations. Comparable to the case of $\theta = 15°$, the location of R2 for an angle of $\theta = 45°$ is found to be shifted to the sideward region that remains in the wake of Island 1 as the island moves into the adjacent sheltered region (*Fig. 22(e)*). An additional feature to note is the location of R2 for an angle of $\theta = 60°$. For the smaller separations considered here of S/d = 2 and S/d = 2.5, R2 is observed to occur on the lee side of the island (*Fig. 20(f)* and *Fig. 21(f)*). This is accounted for by the position of Island 2 in the sheltered regions of both upstream islands, reducing the run-up on the front of the island. At a separation of S/d = 3, however, R2 occurs at the front of the island as this region no longer lies in the shadow of the upstream islands but is exposed directly to the incident wave (*Fig. 22(f)*).

The interaction between the propagating solitary wave and the entirely separated three-island cluster with S/d = 3 and $\theta = 15°$ is characterised in the snapshots of *Figure 24*. Despite R2 being located in the region of Island 2 that lies in the wake of Island 1 for the smaller separations of S/d = 2 and S/d = 2.5, for S/d = 3, the islands are sufficiently separated for the wave to continue propagating past Island 1. R2 is then not just caused by the wake of Island 1, but also by the contribution from the continued action of the wave, giving a large run-up value of R2 at the back of the island (*Fig. 23(c)* and *Fig. 24(g)*). At this separation, the behaviour of the wave as seen in *Figure 24* suggests that the islands effectively act as isolated single islands, each producing a reflected wave and wake with little interaction between the islands. The highest predicted run-up at this separation of 0.0794m for $\theta = 30°$ occurs at Island 3 and is comparable to the maximum run-up height of 0.0793m for the single island.

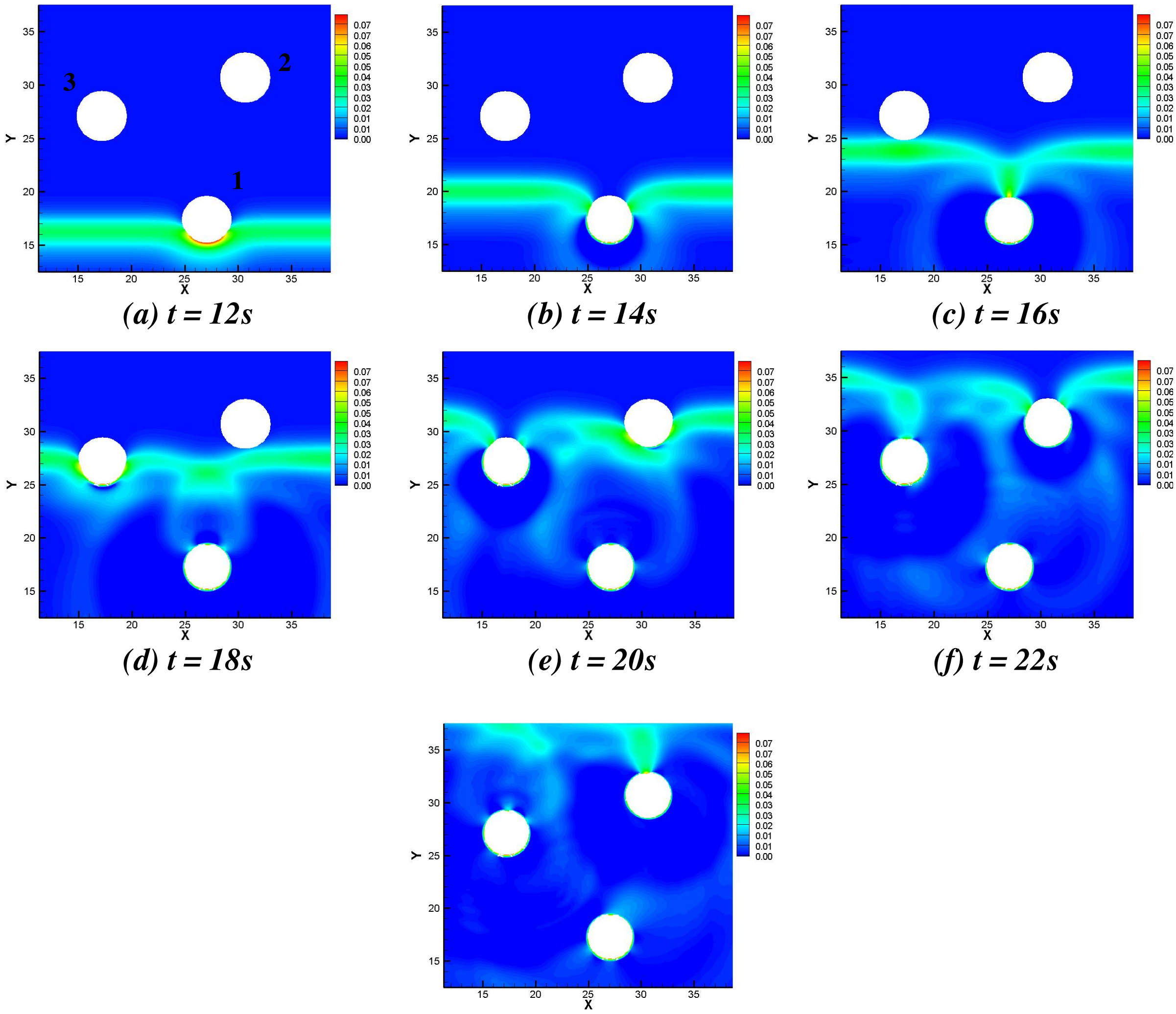

(a) t = 12s *(b) t = 14s* *(c) t = 16s*

(d) t = 18s *(e) t = 20s* *(f) t = 22s*

(g) t = 24s

Fig. 24 Interaction between propagating solitary wave and separated triple-island cluster (S/d = 3, θ = 15°)

6. CONCLUSIONS AND FURTHER WORK

6.1. Conclusions

This project examines the application of the shock-capturing time variation diminishing (TVD) Lax-Wendroff scheme, developed by *Liang (2010)*, to solve the shallow-water Boussinesq-type equations and to model the interaction between a solitary propagating wave, representative of a tsunami event, and clusters of three islands. In this study, the behaviour of the wave is analysed with regards to the maximum run-up height predicted by the model, and the location of its incidence. The accuracy of the numerical model is verified for the case of a single isolated island by comparison with the experimental data of *Liu et al. (1995)*, and is found to provide adequate corroborative evidence for validating the model. It is then assumed that the model is capable of simulating the three-island cluster. The two key parameters of island separation, S/d, and the rotation of the cluster, θ, are defined to characterise the configuration of the island cluster, and the islands are established to be identical in size to simplify the analysis. The influence of these parameters on the maximum run-up heights recorded are examined in the ranges of $1 \leq S/d \leq 3$ and $0° \leq \theta \leq 60°$, in which the island arrangements vary from merged islands at still water level, partially merged islands below still water level and separated islands.

Maximum run-up on the three-island cluster is found to be heavily dependent on S/d and θ, with significantly higher values of run-up than those of the isolated single island test case. Simulations for various island configurations suggest that considerably larger run-up heights are predicted at smaller separations when the islands are merged either at or below still water level. This is attributable to the existence of the narrow channel between the islands when partially merged, which gives rise to reflective, refractive, diffractive, and shoaling effects on the wave, resulting in superposition of waves and therefore higher run-ups in these channel regions. At particularly small separations, the cluster of islands effectively acts as a single entity, producing one wake at the rear of the cluster. At larger separations, however, the islands exhibit behaviour similar to that of individual isolated islands, producing separate wakes, due to the reduced channel effect, permitting the solitary wave to continue to propagate after passing an island. As θ increases, interaction between the islands varies, and the shadow effect can be a significant contribution to the maximum run-up predicted and its location around the island. For separated islands, an increase in θ indicates a shift in the position of the rear island from an exposed sideward location to the sheltered region of the upstream island. As the angle approaches 30°, the rear island moves into the wake of the upstream island, hence experiencing a large run-up height at a point directly in the wake. As the angle is increased further, the rear island then moves back into the adjacent sheltered region, witnessing a decrease in maximum run-up. Meanwhile, the two upstream islands become aligned, taking the direct impact of the propagating wave. At an angle of 60°, the rear island can experience the shadow effect from the two upstream islands, the extent of which is determined by the separation. This noticeable shadow effect governs the magnitude and location of the maximum run-up.

The model for finding the maximum run-up heights on the islands can be used to represent the effects of a real-life tsunami scenario by appropriate methods of scaling. Dimensions such as the water depth, island height and diameter, and wave height can be easily scaled linearly, and as the forces of the water flow are not being examined in this study, it follows that the run-up heights can be easily found for a real-life tsunami wave. The model is hence assumed to be representative of a real tsunami event for the purposes of modelling run-up effects.

6.2. Further work

The interaction between a solitary propagating wave and the three-island cluster can be analysed in further detail by running more simulations for different configurations of island arrangements. As the present results suggest greater surface displacements at smaller island separations, additional simulations can be run at separations of $S/d < 1$ and at smaller intervals, in which the islands are partially merged above the still water level and fully merged. Supplementary simulations can also be run to find the critical value of separation, after which the maximum run-up on Island 2 will decrease and the interaction effect becomes insignificant. At a rotation of $\theta = 30°$, the rear island is located directly behind the upstream island in its wake and is not exposed to the incident wave. Extra simulations can be run at this rotation to find the critical value for which Island 2 is no longer affected by the wake of Island 1. In this study, the three-island cluster is idealised by modelling three islands that are identical in size. However, for the purpose of informing on the likely effects of a real-life tsunami event, this is unlikely to be realistic. Further analysis can therefore be undertaken on islands of varying dimensions and with varying slopes, in addition to waves of varying heights.

Ultimately, the results and analysis presented in this project on the locations and magnitudes of maximum run-up heights are to provide useful information for the planning and implementation of tsunami mitigation actions. It is intended to inform planners and designers with regards to the height to which coastal defence structures are to be designed, and the minimum clearance distance between the shoreline and future construction of coastal settlements, with the aim of minimising the extent of damage caused by these destructive natural hazards.

7. REFERENCES

1. Chen, J. M., and Liang, D., (2012), "Tsunami Wave Run-up on the Clustered Islands using Boussinesq-type Model", *Proceedings of the Twenty-second (2012) International Offshore and Polar Engineering Conference*
2. Wang, X., (2009), "User Manual for COMCOT Version 1.7 (First Draft)", http://ceeserver.cee.cornell.edu/pll-group/comcot_down.htm
3. Liang, D., Lin, B., and Falconer, R. A., (2007), "Simulation of rapidly varying flow using an efficient TVD–MacCormack scheme", *Internal Journal for Numerical Methods in Fluids*, 53:811-826
4. Madsen, P. A., and Sorensen, O. R., (1992), "A new form of the Boussinesq equations with improved linear dispersion characteristics. Part 2. A slowly-varying bathymetry", *Coastal Engineering*, 18(3): 183-204
5. Madsen, P. A., Murray, R., and Sorensen, O. R., (1991), "A new form of the Boussinesq equations with improved linear dispersion characteristics", *Coastal Engineering*, 15: 371-388
6. Liang, D., Borthwick, A. G. L., and Romer-Lee, J. K., (2011), "Run-Up of solitary waves on twin conical islands using a Boussinesq model", *Journal of Offshore Mechanics and Arctic Engineering*, Vol. 134, Issue 1
7. Liu, P. L. -F., Cho, Y., Briggs, M. J., Kanoglu, U., and Synolakis, C. E., (1995), "Run-up of solitary waves on a circular island", *Journal of Fluid Mechanics*, 302:259-285 Cambridge University Press
8. Briggs, M. J., Synolakis, C. E., Harkins, G. S., and Green, D. R., (1995), "Laboratory Experiments of Tsunami Runup on a Circular Island", *Pure and Applied Geophysics*, 144(3-4): pp. 569-593
9. National Oceanic and Atmospheric Administration Centre for Tsunami Research, "Solitary wave on a conical island", http://nctr.pmel.noaa.gov/benchmark/Laboratory/Laboratory_ConicalIsland/index.html
10. US Army Corps of Engineers: Coastal and Hydraulics Laboratory, "Tsunami Benchmark #2: Runup of Solitary Waves on a Circular Island, Tsunami Study", http://chl.erdc.usace.army.mil/chl.aspx?p=s&a=Projects;35

11. Chen, Q., Kirby, J. T., Dalrymple, R. A., Kennedy, A. B., and Chawla, A., (2000), “Boussinesq Modelling of Wave Transformation, Breaking, and Runup”, *Journal of Waterway, Port, Coastal, and Ocean Engineering*, 126(1), pp. 48-56
12. Fuhrman, D. R., and Madsen, P. A., (2008), “Simulation of nonlinear wave run-up with a high-order Boussinesq model”, *Coastal Engineering*, 55:139-154
13. Madsen, P. A., Bingham, H. B., and Liu, H., (2002), “A new Boussinesq method for fully nonlinear waves from shallow to deep water”, *Journal of Fluid Mechanics*, 462:1-30
14. Titov, V. V., and Synolakis, C. E., (1998), “Numerical modelling of tidal wave runup”, *Journal of Waterway, Port, Coastal, and Ocean Engineering*, 124(4): 157-171
15. Wei, Y., Mao, X. Z., and Cheung, K. F., (2006), “Well-balanced finite-volume model for long-wave runup”, *Journal of Waterway, Port, Coastal, and Ocean Engineering*, 132(2): 114-124

8. APPENDIX A

8.1. MATLAB script for single island

```
clear;

%set variables
rb=3.6;             %bottom radius
rt=1.1;             %top radius
swd=0.32;           %still water depth
grad=0.25;          %slope gradient
rm=rb-(swd/grad);   %mid radius at still water level
height=0.625;       %island height
m=25;               %x position of island centre
deltax = 0.05;      %grid x spacing
xend = 50;
n=25;               %y position of island centre
deltay = 0.05;      %grid y spacing
yend = 50;

%number of iterations
iend=(xend/deltax)+1;
jend=(yend/deltay)+1;

%create storage
z=zeros(iend,jend);
h=zeros(iend,jend);                     %still water depth
eta=zeros(iend,jend);                   %free-surface displacement

x=((1:iend)-1).*deltax;
y=((1:jend)-1).*deltay;

for i=1:iend
    for j=1:jend

    d = sqrt((m-x(i))^2+(n-y(j))^2);
     %distance to island centre

        if d > rb
            z(i,j) = -swd;
            eta(i,j) = 0;
        elseif d > rm && d < rb
            z(i,j) = -(swd-(rb-d)*grad);
            eta(i,j) = 0;
        elseif d > rt && d < rm
            z(i,j) = (rm-d)*grad;
            eta(i,j) = z(i,j);
        else
            z(i,j) = height-swd;
            eta(i,j) = z(i,j);
        end
```

```
        h(i,j) = -z(i,j);

    end
end

save('islandh.mat','h')

save('islandeta.mat','eta')

surf(x,y,z);
```

8.2. MATLAB script for three-island cluster

```
clear;

%set variables
rb = 3.6;                   %bottom radius
rt = 1.1;                   %top radius
swd = 0.32;                 %still water depth
grad = 0.25;                %slope gradient
rm = rb-(swd/grad);         %mid radius at still water level
height = 0.625;             %island height
m = 25;                     %x coordinate of centre of cluster
deltax = 0.05;              %grid x spacing
xend = 50;
n = 25;                     %y coordinate of centre of cluster
deltay = 0.05;              %grid y spacing
yend = 50;
theta = (5/180)*pi;         %angle of rotation in radians
s = 5.8;                    %island separation

%number of iterations
iend = (xend/deltax)+1;
jend = (yend/deltay)+1;

%create storage
z = zeros(iend,jend);
h = zeros(iend,jend);                   %still water depth
eta = zeros(iend,jend);                 %free-surface displacement

x1 = m+((sqrt(3)*s/3)*sin(theta));   %x-coordinate of island 1
y1 = n-((sqrt(3)*s/3)*cos(theta));   %y-coordinate of island 1

x2 = m-((sqrt(3)*s/3)*sin(theta-(pi/3)));
%x-coordinate of island 2
y2 = n+((sqrt(3)*s/3)*cos(theta-(pi/3)));
%y-coordinate of island 2

x3 = m-((sqrt(3)*s/3)*sin((2*pi/3)-theta));
%x-coordinate of island 3
y3 = n-((sqrt(3)*s/3)*cos((2*pi/3)-theta));
%y-coordinate of island 3
```

```
x = ((1:iend)-1).*deltax;          %x-coordinate of grid point
y = ((1:jend)-1).*deltay;          %y-coordinate of grid point

for i = 1:iend
    for j = 1:jend

        d1 = sqrt(((x1-x(i))^2)+((y1-y(j))^2));
          %distance between grid point and centre of island 1
        d2 = sqrt(((x2-x(i))^2)+((y2-y(j))^2));
          %distance between grid point and centre of island 2
        d3 = sqrt(((x3-x(i))^2)+((y3-y(j))^2));
          %distance between grid point and centre of island 3

        d = [d1 d2 d3];

        dmin = min(d);
          %distance between grid point and centre of nearest
          island

        if dmin > rb
            z(i,j) = -swd;
            eta(i,j) = 0;
        elseif dmin > rm && dmin < rb
            z(i,j) = -(swd-(rb-dmin)*grad);
            eta(i,j) = 0;
        elseif dmin > rt && dmin < rm
            z(i,j) = (rm-dmin)*grad;
            eta(i,j) = z(i,j);
        else
            z(i,j) = height-swd;
            eta(i,j) = z(i,j);
        end

        h(i,j) = -z(i,j);

    end
end

save('3islandh.mat','h')

save('3islandeta.mat','eta')
```

8.3. Risk assessment retrospective

The risk assessment completed prior to the commencement of the project, identifying the possibility of hazards associated with long periods of computer use, was found to be an accurate reflection of the hazards actually encountered during the course of the project. For this reason, in retrospect, the process of assessing risk would not be modified.